


April 2020

## Manipulation and Patterning of Mammalian Cells Using Vibrations and Acoustic Forces

Joel Cooper  
*University of South Florida*

Follow this and additional works at: <https://scholarcommons.usf.edu/etd>

 Part of the [Acoustics, Dynamics, and Controls Commons](#), and the [Biomedical Engineering and Bioengineering Commons](#)

---

### Scholar Commons Citation

Cooper, Joel, "Manipulation and Patterning of Mammalian Cells Using Vibrations and Acoustic Forces" (2020). *Graduate Theses and Dissertations*.  
<https://scholarcommons.usf.edu/etd/8178>

This Dissertation is brought to you for free and open access by the Graduate School at Scholar Commons. It has been accepted for inclusion in Graduate Theses and Dissertations by an authorized administrator of Scholar Commons. For more information, please contact [scholarcommons@usf.edu](mailto:scholarcommons@usf.edu).

Manipulation and Patterning of Mammalian Cells Using  
Vibrations and Acoustic Forces

by

Joel Cooper

A dissertation submitted in partial fulfillment  
of the requirements for the degree of  
Doctor of Philosophy  
Department of Mechanical Engineering  
College of Engineering  
University of South Florida

Co-Major Professor: Nathan Gallant, Ph.D.  
Co-Major Professor: Rasim Guldiken, Ph.D.  
Daniel Hess, Ph.D.  
Garrett Matthews, Ph.D.  
Ryan Toomey, Ph.D.

Date of Approval:  
April 12, 2020

Keywords: Faraday Waves, Resonance, Fluorescent Microscopy, Atomic Force Microscopy,  
Tissue Engineering

Copyright © 2020, Joel Cooper

## **Dedication**

I would like to dedicate this dissertation to my amazing family, friends, and loved ones. Their love and support throughout this journey made this work possible. They were always there when I needed them, laughing with me through good times and helping me push through the bad times.

## **Acknowledgments**

I would like to express my deepest appreciation to my advisors, Dr. Nathan Gallant and Dr. Rasim Guldiken. This dissertation would not have been possible without their guidance, support, and endless patience over the years. I am forever grateful to both of them for everything they have done.

I would also like to thank the members of my committee for their invaluable advice throughout my time here at USF. Dr. Daniel Hess who was always willing to share his insights and understanding of vibrations. Dr. Ryan Toomey who helped broaden my knowledge of polymers. Dr. Garrett Matthews who provided valuable knowledge of AFM.

I acknowledge and am grateful for the National Science Foundation. During my degree I received support under NSF GRFP, GROW, and EAPSI. Through GROW and EAPSI, I was able to live in Nagoya, Japan and conduct international collaborative research. I learned so much through this experience and am truly grateful.

To my fellow students from the Cellular Mechanotransduction and Biomaterials Lab and the Microfluidics and Acoustics Lab, both past and present, thank you all for your support, collaboration, and friendship.

Finally I would like to thank my family and friends for their unconditional love and constant support. They were with me every step of the way.

## Table of Contents

List of Tables .....	iii
List of Figures .....	iv
Abstract .....	vii
Chapter 1: Introduction .....	1
Chapter 2: Manipulation of Cell Attachment and Viability via Insonification .....	4
2.1 Background .....	4
2.2 Experimental Design .....	6
2.2.1 Cell Culture and Reagents .....	6
2.2.2 Automated Fluorescent Microscopy Analyses .....	6
2.2.3 Acoustic Manipulation Experiment Protocol .....	7
2.2.4 Statistical Analysis .....	10
2.3 Results .....	10
2.3.1 Effects of Insonification on Cell Attachment .....	10
2.3.2 Effects of Insonification on Cell Viability .....	14
2.3.3 Effects of Distance from Source of Acoustic Excitation on Cell Attachment .....	16
2.4 Conclusions .....	18
Chapter 3: Manipulation and Patterning of Cells using Acoustic Forces .....	20
3.1 Background .....	20
3.2 Computer Modeling and Experimental Validation .....	21
3.3 Methods and Experimental Setup .....	23
3.3.1 Cell Culture and Reagents .....	23
3.3.2 Cell Manipulation .....	24
3.3.3 Automated Fluorescent Microscopy Analyses .....	25
3.3.4 Macro Fluorescent Image Analyses .....	26
3.4 Results and Discussion .....	26
3.4.1 Simulation Validation .....	26
3.4.2 Cell Pattern Characterization using Macro Images .....	29
3.5 Conclusion and Future Work .....	54

Chapter 4: Key Findings and Future Work.....	56
4.1 Incomplete and Ongoing Work: Characterization of Cellular Mechanical Properties using AFM.....	57
4.1.1 Background.....	57
4.1.1.1 Cell Mechanical Properties: Elasticity and Natural Frequency.....	58
4.1.1.2 Cytoskeletal Composition and Cell Shape.....	59
4.1.1.3 Objectives .....	60
4.1.2 Methods and Materials.....	61
4.1.2.1 Cell Culture and Reagents .....	61
4.1.2.2 Fabrication of Microcontact Printing Stamp.....	62
4.1.2.3 Microcontact Printing Procedure .....	63
4.1.2.4 Experimental Procedure.....	65
4.2 Limited Results .....	67
4.2.1 Microcontact Printing Direct Proteins .....	67
4.2.2 ESEM Analysis of Mammalian Cells .....	68
4.3 Conclusion and Future Work .....	69
4.3.1 Future Work: AFM and Cytoskeletal Inhibitors.....	69
References.....	71
Appendix A Copyright Permissions .....	76

## List of Tables

Table 1 SolidWorks vs Ansys modal simulation results for a 100mm polystyrene tissue culture dish .....	27
Table 2 Longitudinal measurements of the distance between the center of the bands of cells for 40Hz on Day 1.....	37
Table 3 Longitudinal measurements of the distance between the center of the bands of cells for 40Hz on Day 2.....	37
Table 4 Longitudinal measurements of the distance between the center of the bands of cells for 40Hz on Day 3.....	37
Table 5 Longitudinal measurements of the distance between the center of the bands of cells for 75Hz on Day 1.....	37
Table 6 Longitudinal measurements of the distance between the center of the bands of cells for 75Hz on Day 2.....	38
Table 7 Longitudinal measurements of the distance between the center of the bands of cells for 75Hz on Day 3.....	38

## List of Figures

Figure 1. Schematic representation of experimental setup. ....	7
Figure 2 Representative macro images of fluorescently labeled cells before and after insonification with maximum or minimum energy for high and low power.....	10
Figure 3 The percent of cells remaining attached (a) 1 h or (b) 24 h after sonication at various power and energy values.....	11
Figure 4. The percent of viable cells (a) 1 h or (b) 24 h after insonification at various power and energy levels. ....	14
Figure 5. Relation between acoustic intensity and cell detachment after exposure to a power of 3 watts and energy of 3 joules (3W3J). ....	16
Figure 6 SolidWorks modal frequency simulation results compared to experimental modal frequencies. ....	22
Figure 7 10 $\mu$ m polystyrene spheres in 5ml of DI H <sub>2</sub> O at 75Hz.....	28
Figure 8 Macro image of green fluorescent NIH3T3 fibroblasts during vibrational patterning at 40Hz.....	29
Figure 9 Macro image of NIH3T3 fibroblasts after patterning at 40Hz. ....	29
Figure 10 Macro image of NIH3T3 fibroblasts after patterning at 40Hz. ....	30
Figure 11 Macro image of NIH3T3 fibroblasts at 40 Hz with increased amplitude. ....	31
Figure 12 Representative image of NIH3T3 Fibroblasts patterned at 40Hz. ....	33
Figure 13 Representative image of NIH3T3 Fibroblasts patterned at 75Hz. ....	34
Figure 14 Representative image of distance measurements ....	36
Figure 15 Average distances and standard deviations between bands of cells over time.....	38
Figure 16 Representative fluorescent intensity vs location for 40Hz. ....	39
Figure 17 Combined fluorescent intensity data for 40Hz 4 hours after patterning ....	41
Figure 18 Combined fluorescent intensity data for 75Hz 4 hours after patterning ....	41



Figure 19 40Hz 4 hours after patterning .....	42
Figure 20 40Hz 4 hours after patterning .....	43
Figure 21 40Hz 4 hours after patterning .....	43
Figure 22 40Hz 4 hours after patterning .....	44
Figure 23 40Hz 4 hours after patterning .....	44
Figure 24 40Hz 24 hours after patterning .....	44
Figure 25 40Hz 24 hours after patterning .....	45
Figure 26 40Hz 24 hours after patterning .....	45
Figure 27 40Hz 24 hours after patterning .....	45
Figure 28 40Hz 24 hours after patterning .....	46
Figure 29 40Hz 48 hours after patterning .....	46
Figure 30 40Hz 48 hours after patterning .....	46
Figure 31 40Hz 48 hours after patterning .....	47
Figure 32 40Hz 48 hours after patterning .....	47
Figure 33 40Hz 48 hours after patterning .....	48
Figure 34 75Hz 4 hours after patterning .....	48
Figure 35 75Hz 4 hours after patterning .....	48
Figure 36 75Hz 4 hours after patterning .....	49
Figure 37 75Hz 4 hours after patterning .....	49
Figure 38 75Hz 4 hours after patterning .....	49
Figure 39 75Hz 24 hours after patterning .....	50
Figure 40 75Hz 24 hours after patterning .....	50
Figure 41 75Hz 24 hours after patterning .....	50
Figure 42 75Hz 24 hours after patterning .....	51
Figure 43 75Hz 24 hours after patterning .....	51

Figure 44 75Hz 48 hours after patterning. ....	51
Figure 45 75Hz 48 hours after patterning. ....	52
Figure 46 75Hz 48 hours after patterning. ....	52
Figure 47 75Hz 48 hours after patterning. ....	52
Figure 48 75Hz 48 hours after patterning. ....	53
Figure 49 Fabrication of microcontact printing stamp and stamping procedure. ....	62
Figure 50 Surfcoorder ET200 used to verify etch depth of photoresist.....	63
Figure 51 Nano-robotic manipulation system inside ESEM .....	65
Figure 52 ESEM images of AFM cantilever calibration. ....	65
Figure 53 Green fluorescent fibronectin stamped onto a clean glass slide.....	67
Figure 54 Successfull cell attachment to fibronectin islands.....	67
Figure 55 NIH3T3 fibroblast imaged using ESEM. ....	68
Figure 56 ESEM cell elasticity using tipless AFM cantilevers. ....	69

## Abstract

Recently, there has been a surge in researchers and scientists investigating different methods which move, manipulate, and pattern biological cells. Multiple different mechanisms can be used for cellular manipulation, microfluidics, biochemical queues, and even optics, just to name a few. However, all techniques have their downsides. A majority of these methods require expensive equipment or reagents and can only manipulate a small number of cells at a time.

Some of the most common cell manipulation devices utilize acoustic pressure waves to move the cells to desired locations. Currently, it is unknown what level of force from these types of devices a biological cell can withstand before irreparable damage occurs. The first section of this dissertation investigates this issue. Briefly, this study found that the power into the acoustic device, cell exposure time to the acoustic waves and the distance from the source of the acoustic wave generator all effect cell attachment and viability. These results aid in providing a better understanding of the acoustic pressures a cell can withstand before permanent damage occurs.

The core of the research described in this dissertation investigates a new method of cell manipulation and patterning. This new method utilizes standing waves, generated by an inexpensive mechanical vibrator, to manipulate cells into the mode shapes of the container the cells are within.

NIH3T3 Fibroblasts were successfully patterned using the frequencies 40Hz and 75Hz and the overall pattern persisted for over 48 hours. Further investigations confirmed that the

patterning method described here had no noticeable negative effects on cell viability, proliferation, or migration. The results of this research provide a fast, flexible, and inexpensive method for manipulating and patterning large numbers of cells.

## Chapter 1: Introduction

One of the biggest dilemmas in tissue engineering currently is the development of proper 3D vasculature throughout engineered tissues [1]. Vasculature is critical to the success of an implanted constructed tissue as it is required for sufficient nutrient, oxygen and waste transport to and from cells within the structure. Without access to a vascular network, cells outside the diffusion limit [1, 2] will develop a buildup of metabolic waste and be starved of nutrients; this combination can lead to cell death and eventual failure of the implant [1]. Previously it has been shown that the body responds to an implanted tissue by developing its own vascular network throughout; however, this is a slow process and cannot be relied upon for successful implant integration.

Optimal integration of this network must mimic the function and structure of vasculature in native tissues an implant is attempting to replace. This means the engineered vascular network must be distributed throughout the tissue similar to capillaries, connect to larger vessels acting as veins and arteries, and have locations where the host's native vasculature can be connected through surgical means [1-3]. Knowing this, tissue engineers have begun developing methods for creating vasculature in an engineered tissue in vitro. These methods include biodegradable and decellularized scaffolds, cell self-assembly, perfusable microvascular networks, and many others [3]. Each of these techniques has their disadvantages. For example biodegradable scaffolds with polymer remnants can degrade the mechanics of tissue [4] and cell self-assembly has been shown to unroll during high blood flow [5]. While these methods of developing vasculature do have their benefits, it is clear that new techniques should still be investigated.

This research focuses on manipulating the spatial organization of cells to rapidly form patterned layers of cells. Ultimately this novel method could enable the formation of complex structures such as vasculature without the use of biomaterials or expensive specialized equipment. The cell manipulation method discussed in this paper stems from cymatics, a subset of modal vibrations. Vibrational and acoustic forces, induced by a simple mechanical wave driver and signal generator, act on the cells suspended in media and force the cells to move to nodal locations. However, the interaction between acoustic forces and biological cells is a relatively recent research topic and there are multiple gaps in the current literature. In order to successfully utilize acoustic forces in cell manipulation, these gaps must be investigated.

First, there has been little investigation into both the immediate and long-term effects of acoustic forces on cell viability. Previous acoustic particle manipulation studies have shown that small forces generated by interdigital transducers can move particles and cells in suspension but cannot generate enough force to detach adherent cells [6-9]. It is also known that very large acoustic forces can cause cavitation which destroys cell membranes, effectively killing the cell. The research described in this section delves into the intermediate range of acoustic pressure waves and attempts to shed light on two main questions: (1) how much acoustic force cells can handle without obtaining permanent damage and (2) how much acoustic force is required to detach cells from a normal tissue culture dish.

The second section, and main portion of this research, focuses on the manipulation and patterning of cells in common polystyrene tissue culture dishes using only vibrational and acoustic forces. Preliminary work has proven the importance of computer modeling for accurate prediction of the parameters required to achieve specific patterns. Insights gained from the previous section aids in the development of these computer models and experimental data is be

used to verify accuracy. This section delves into successful cell patterning and analyses long term cell viability, pattern retention over time; ensuring this new method of cellular manipulation is practical for researchers worldwide.

Finally, it is known that the acoustic force acting on a particle in suspension varies based on the compressibility of the particle [10]. Unlike microbeads used in a majority of acoustic manipulation studies, biological cells are heterogeneous in structure and mechanical properties of the cell can change depending on a multitude of factors. This is due to the ever-changing internal components of the cell's cytoskeleton and its response to stimuli. Current literature discussing the cell's mechanical properties, including compressibility measurements, only probe minimally into the cell's surface correlating to local stiffness values [11-14]; yet quantification of acoustic force on a cell requires the overall or global stiffness. This section discusses ongoing and future work which will lead to the measurement of two physical properties of cells: (1) global cellular compressibility and (2) global cellular natural frequency, a property which has previously been ignored in the literature but is important when working with acoustics. Additionally, this section discusses the possible contribution of the shape of the cell as well as specific cytoskeletal elements to its overall, or global, mechanical properties.

## **Chapter 2: Manipulation of Cell Attachment and Viability via Insonification**

### **2.1 Background**

Manipulation of bio-particles and live cells is crucial to a variety of biomedical applications, including diagnostics and fundamental studies of cell-cell interactions [7, 15-19]. In recent decades, interest has grown in the use of acoustic devices, mostly in the ultrasound range, to manipulate, pattern, or alter biological cells. While there have been several successful approaches [7, 9, 20-28], only a few investigated cell viability after ultrasonic exposure [25, 29-31]. Additionally, these in vitro studies only examined cells in suspension, and none attempted to use acoustic devices to manipulate or alter cells adhered to a substrate. Currently, there is a gap in the understanding of how adhered cells are affected by exposure to acoustic excitations large enough to detach the cell from the surface.

Therapeutic ultrasound has a long history [24, 27, 32, 33], however the use of acoustics for cellular manipulation was not reported until the 1970s by Dyson et al. [34]. This work revealed that a stationary wave field excited from an ultrasonic transducer could suspend blood cells flowing through the vessels of chick embryos. Notably, further investigation revealed that the plasma membranes of the endothelial cells lining these vessels had been damaged, producing a similar effect to thrombosis [35]. These studies helped spark an interest in using ultrasound for bio-manipulation techniques.

Modern ultrasonic transducers used in bio-manipulation operate at relatively low input power, ranging from 0.5W to 1.5 W, resulting in 100 pN scale forces applied to the particle or cell [7, 20, 36]. These sub-nN scale forces have proven to be suitable for manipulating particles



in static fluid; however, studies have shown that as flow rates increase, acoustic trapping forces are overcome, and guided movement efficiency decreases [20, 37]. This decrease in efficiency can be addressed by increasing the input power to the transducer, correlating to a larger force restraining the particle [20, 37]. Large forces can distort, damage, or even destroy a cell; therefore, it is important to determine the range of acoustic excitations that expose cells to forces which they can withstand without suffering permanent damage.

Current acoustic manipulation techniques are typically only used on cells suspended in fluid media and not applied to cells adhered onto a surface. We have previously showed that an approximately 200 nN adhesive force must be overcome to detach individual fibroblasts [38, 39]. This is orders of magnitude higher than previously reported acoustic forces on cells in suspension [6, 7, 36]. It is clear that acoustic transducers must generate at least 1000 times as much force compared to those in current use, while not irreversibly disrupting cellular integrity if they are to be used to manipulate adherent cells. The development of more powerful therapeutic devices and cell manipulation techniques utilizing acoustic transducers requires further investigation of the effects of insonification on cell attachment and viability.

In this study, these relationships were investigated by using a sonication probe, a device commonly used for cell lysis, which operates at the low end of ultrasonic frequencies, as a simple tool for acoustic excitation of adherent cells. Adherent cells were insonified over a range of 3 to 48 J while varying the power and duration of acoustic excitation. The findings presented here demonstrate that the power output from the sonicator, the exposure time, and the acoustic intensity all play a role in cell detachment and regulating viability.

## 2.2 Experimental Design

### 2.2.1 Cell Culture and Reagents

NIH3T3 murine embryonic fibroblasts (CRL-1658, ATCC) were cultured in complete growth medium (CGM) containing 10% newborn calf serum and 1% penicillin-streptomycin in Dulbecco's modified Eagle's medium. Cells were passaged every three days, using 0.25% trypsin-EDTA and used between passages 5 and 20. Cells were labeled with 3 $\mu$ M calcein-AM suspended in Dulbecco's phosphate-buffered saline containing calcium and magnesium (DPBS). The initially non-fluorescent calcein AM penetrates the cellular membrane where intracellular esterases within living cells hydrolyze acetoxymethyl ester, producing a green fluorescence in the cytoplasm. This fluorescence is only retained in live cells and quickly dissipates if the cell's membrane is compromised [40, 41]. Cell culture reagents were purchased from Invitrogen unless otherwise noted.

### 2.2.2 Automated Fluorescent Microscopy Analyses

Cell attachment and spatial distribution analyses in each sample were performed using an Eclipse Ti-U (Nikon Instruments) inverted microscope equipped with a CCD camera (CoolSNAP HQ2 Photometrics) and appropriate fluorescent filter sets. Automated fluorescence microscopy, controlled by NIS-Elements software (version 4.20, Nikon Instruments), was used to quantify cell number and distribution in each experiment. This automation used a computer-controlled stage, in conjunction with the microscope setup described above, to capture fluorescent images at 73 different x-y locations on each dish for a total analyzed area of 87.5 mm<sup>2</sup> (9% of total dish area). The number of cells at each location was recorded.

### 2.2.3 Acoustic Manipulation Experiment Protocol

Cells were seeded 16 hours before the experiment at 100 cells/mm<sup>2</sup> onto 35mm sterile tissue culture polystyrene (TCP) dishes (Corning). This time was chosen so cells would attach and fully spread but not proliferate appreciably before insonification [38, 42]. During this time, the cells were incubated at 75% relative humidity, 5% CO<sub>2</sub>, and 37°C. The next day the media was aspirated, and the cells were rinsed with 2ml DPBS. Fluorescent labeling of live cells was achieved by adding 0.75ml of 3μM calcein AM to each dish, which were then incubated for 30 minutes. Following labeling, the cells were washed with DPBS, and 2ml of fresh CGM was added to each dish. Samples were individually imaged and analyzed using the previously described automated fluorescent microscopy technique to determine the average cell density and cell distribution information prior to insonification.

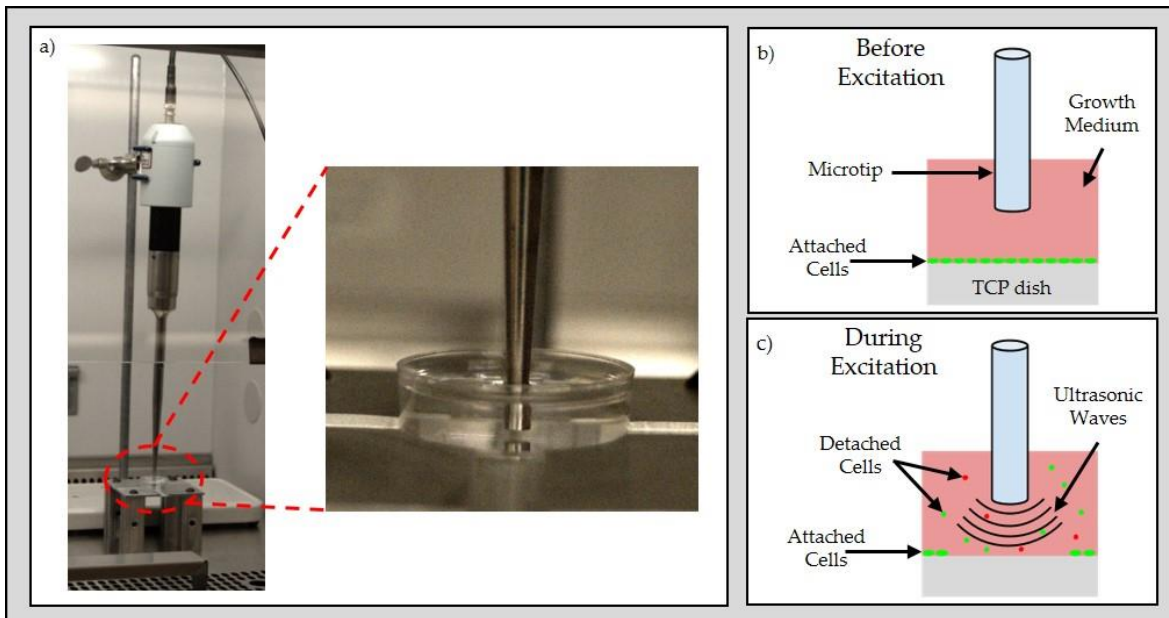


Figure 1. Schematic representation of experimental setup. (a) Sonicator probe with microtip horn attachment inside biosafety cabinet with close up of microtip probe submerged in a 35mm diameter tissue culture polystyrene (TCP) dish. (b) Before excitation, the microtip was submerged in the TCP dish containing growth media and living cells attached to the surface of the dish. (c) During excitation, the sonicator is activated and the microtip insonifies the region. Green and red particles represent alive and dead cells, respectively.

After initial imaging, 4ml of additional fresh CGM was added to each dish. This was done per operation manual recommendations to operate below the cavitation region [43]. Cells were then exposed to one of four power settings (3W, 6W, 9W, or 15W) for varied time intervals (1s to 15s) to obtain a range of total energy inputs (3 joules to 48 joules) as calculated by equation (1) below. A Misonix Sonicator 3000 (Cole-Parmer), equipped with a 1/8 inch micro-tip horn that operates at 20 kHz and vibrates in the longitudinal direction [43], was used to generate the desired acoustic excitation in each experiment from a fixed position 2mm above the dish surface Figure 1. This unfocused sonication probe is capable of generating an intermediate range of acoustic intensities representing the gap between microtransducers, generating 0.05 W/cm<sup>2</sup> [7] to 1 W/cm<sup>2</sup> [44], and high-intensity therapeutic devices, which typically generate several W/cm<sup>2</sup> to orders of magnitude more [45, 46]. Cellular damage due to cavitation was considered; however, this effect was minimized by maintaining a 2mm gap between the fully submerged probe tip and the cells on the surface of the dish. Sonication devices are known to generate heat, so the temperature was recorded using a thermal probe (SD-3007 Reed Instruments) to ensure the dish never exceeded 40 °C, which is generally regarded as safe for mammalian cells [47].

$$\text{Energy (J)} = \text{Power (W)} * \text{Time (s)} \quad (1)$$

Immediately after insonification, the medium, containing cells which had detached from the plate, was carefully transferred from the original dish to a new sterile 35mm tissue culture dish, and 2ml of fresh CGM was carefully dispensed into the original dish. This allowed differentiation between cells which remained attached, cells destroyed during insonification, and cells detached from the plate but survived. Each sample, now consisting of an original dish and a re-plated dish, was incubated at 37°C for 1 hour to allow the detached cells to adhere to the new

dish [38, 42] before the second round of microscopic imaging and analysis. After imaging, 4ml of media was removed from the re-plated dishes to allow for proper O<sub>2</sub> diffusion. Each dish was then incubated overnight under standard culture conditions. The medium was aspirated 24 hours after the initial imaging, and each dish was rinsed with 2ml DPBS before re-labeling with calcein-AM for 30 min. Following this final incubation, samples were washed with DPBS, and 2ml of fresh CGM was added to each dish. Each sample was then imaged and quantified a third and final time.

Following this procedure, the data consisted of the number and distribution of cells in each dish at three unique time points: before exposure (BE), immediately after exposure (AE), and 24 hours after initial imaging. Considering the latter two time points contain data from both the (1) original and (2) re-plated dishes, this analysis provides a total of five unique sets of data for each sample. The number of cells contained in each data set was averaged and divided by the analysis area to determine cell density in cells/mm<sup>2</sup>. To account for variations in cell seeding density, attachment, and viability data were normalized to respective “before exposure” cell densities. Percent cell attachment and viability were determined immediately after exposure by the following equations.

$$\% \text{ Cells Attached} = \frac{\text{AE (1)}}{\text{BE}} * 100 \quad (2)$$

$$\% \text{ Viable Cells} = \frac{[\text{AE (1)} + \text{AE (2)}]}{\text{BE}} * 100 \quad (3)$$

Similarly, cell attachment and viability 24 hours after exposure were determined by substituting data gathered 24 hours after initial imaging into the above equations for AE.

## 2.2.4 Statistical Analysis

Data are reported as mean values  $\pm$  standard deviation of three independent experiments, each performed in triplicate. Statistical comparisons, performed using SigmaPlot 11.2 software, were based on analysis of variance and the Holm-Sidak post hoc test for multiple pairwise comparisons, with a p-value  $< 0.05$  considered significant.

## 2.3 Results

### 2.3.1 Effects of Insonification on Cell Attachment

Significant forces are required to detach adherent and well-spread cells [16]. The effect of acoustic excitation from a sonic transducer on cell adhesion was investigated using a sonication horn adjusted to various power and total energy levels. Figure 2 contains representative macro images of four different 35mm TCP dishes before and after insonification. Before exposure, cells were fully attached and uniformly distributed over each dish surface. After exposure, the distribution of cells that remained attached varied depending on power, energy, and distance from the excitation source.

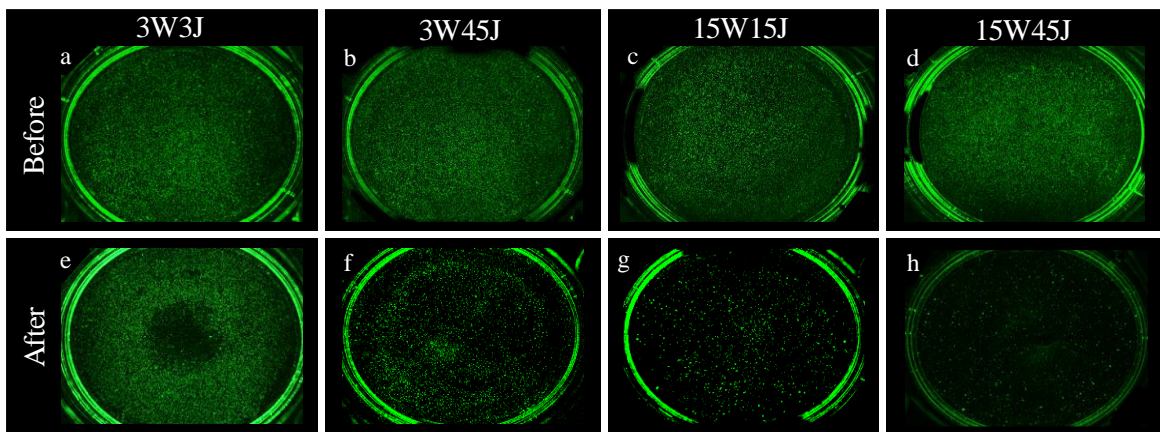


Figure 2 Representative macro images of fluorescently labeled cells before and after insonification with maximum or minimum energy for high and low power. Before excitation, cells were fully attached and uniformly distributed over each dish surface (a-d). Unique distributions arose for cells remaining attached after exposure to (e) 3 watts and 3 joules (3W3J), (f) 3 watts and 45 joules (3W45J), (g) 15 watts and 15 joules (15W15J), or (h) 15 watts and 45 joules (15W45J). Live cells fluorescently labelled with calcein AM were adhered in 35mm diameter tissue culture polystyrene (TCP) dishes.

Cells insonified at the lowest power setting, 3 watts, coupled with the lowest energy, 3 joules, resulted in a distinct radial cell distribution. The lack of fluorescence at the center of the dish indicates significant cell detachment from the surface at radial distances near the excitation source, while cells located further from the center remained adhered to. Using the same power but increasing energy exposure to 45 joules yielded a very different result. At this combination of power and energy dose, a majority of cells were uniformly detached from the surface. The only difference was an increase in energy (extended duration), suggesting a correlation between energy levels and cell attachment. On the higher end of the power spectrum (15 watts), energy levels affected cell adhesion to a lesser degree; exposure to either 15 or 45 joules caused significant cell detachment. The representative images in Figure 2 can also be used to compare samples with similar energy levels but different power inputs. Cells exposed to 45 joules using powers 3 or 15 watts were similar in that a majority of cells detached.

Analyzing a range of energy and power inputs further suggests that the power and energy of the acoustic excitation strongly modulate cell attachment Figure 3. Using equation (2), the

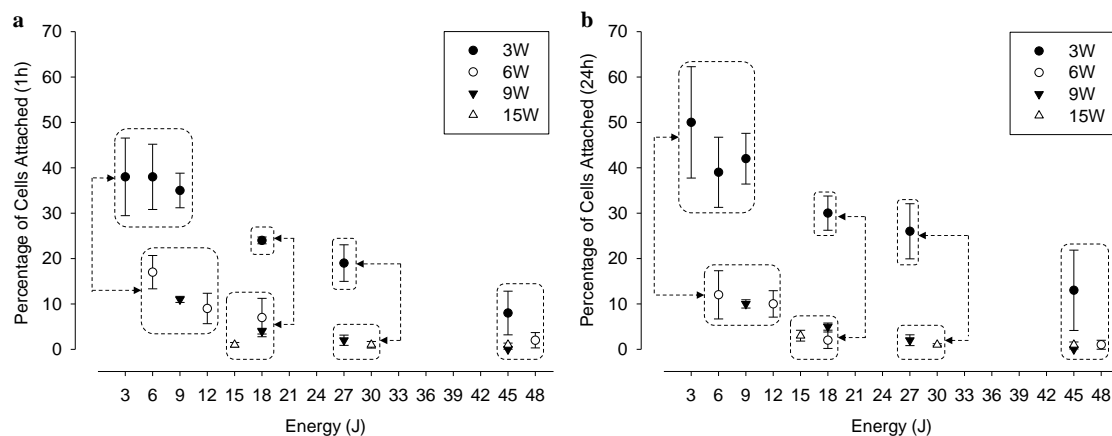


Figure 3 The percent of cells remaining attached (a) 1 h or (b) 24 h after sonication at various power and energy values. Data points grouped within dashed boxes show no significant differences among each other ( $p > 0.05$ ). Groups of data with significant differences ( $p < 0.05$ ) among power series for similar energy ranges are indicated with dashed arrows.

percent of cells remaining attached 1 hour after being insonified and 24 hours after initial imaging were determined. Data points grouped inside of dashed boxes in Figure 3 and Figure 4 showed no significant differences among each other ( $p>0.05$ ), while groups of data with significant differences ( $p<0.05$ ) for similar energy levels are denoted using dashed arrows.

One hour after insonification, the lowest power setting, 3 watts, had a significantly higher percentage of cells remain attached compared to the other power settings up to 45 joules. At 45 joules, cell adhesion was reduced to below 10% for all power levels. The 3-watt input also induced the largest decrease in the attachment as energy was increased, ranging from an average of 39% remaining attached at 3 joules and decreasing down to an average of 8% remaining attached at 45 joules. In contrast, the highest power setting, 15 watts, detached nearly all the cells for all the energy levels tested. These results are consistent with a previous report which concluded that as the power of the acoustic excitation increases, the percent of cells detached from the surface also increases [48].

The 3, 6, and 9-watt power settings had significant differences in the percent of cells remaining attached at different energy levels within each respective series; however, the 15-watt power setting shows no significant differences as few cells remained at all energy levels. The 3-watt series had significant differences in the percent of cells remaining attached at the following energy values: 3 joules and 27 joules ( $p=0.041$ ), 3 joules and 45 joules ( $p=0.008$ ), 6 joules and 27 joules ( $p=0.038$ ), 6 joules and 45 joules ( $p=0.008$ ), 9 joules and 45 joules ( $p=0.024$ ). The 6-watt series had significant differences in the percent of cells remaining attached at 6 joules and 48 joules ( $p=0.008$ ). The 9-watt series had significant differences ( $p<0.05$ ) in the percent of cells remaining attached at all energy values except between 27 joules and 45 joules. These significant trends demonstrate that relatively low power acoustic excitations (3 – 9 W) can detach more cells



from the surface by merely increasing the energy into the system. The facts that few cells remained attached and that there were no significant differences within the 15W series suggests that there is a threshold acoustic power which detaches most of the cells from the surface regardless of the energy input.

Similar trends were observed after allowing cells to recover for 24 hours. That is, following the lowest power exposure, 3 watts, a significantly higher percentage of cells remain attached when compared to the other power series. Again, this difference disappeared when the total energy input reached 45 joules, where none of the power settings were significantly different from each other in terms of cell adhesion.

Data collected 24 hours after the initial imaging showed there were significant differences in the fraction of cells attached at different energy levels within the 3, 9, and 15-watt power settings. The 3-watt series had significant differences in the fraction of cells remaining attached at 3 joules and 45 joules ( $p < 0.001$ ) and 9 joules and 45 joules ( $p = 0.014$ ). The 9-watt series had significant differences ( $p < 0.05$ ) in the fraction of cells remaining attached at all energy values except between 27 joules and 45 joules. The 15-watt series had a significant difference only between the 15 joules and 30 joules ( $p = 0.031$ ) settings.

Healthy NIH3T3 fibroblasts have a doubling time of approximately 20 hours. Comparing the cell count with the corresponding data 24 h later showed that there were no statistically significant increases or decreases in the number of cells remaining attached over 24 hours; therefore, these populations did not follow this standard doubling time. This suggests that the acoustic excitation either disrupted internal cellular mechanisms responsible for the proliferation, or some cells were damaged beyond repair, dying at a rate similar to those proliferating. While not statistically significant, there were minimal increases and decreases in the percent of cells

over 24 hours. Specifically, the 3-watt series tended to increase, whereas the 6, 9, and 15-watt series all tended to decrease, suggesting that long term survival and proliferation of cells which remained attached after insonification largely depends on the power of the excitation.

### 2.3.2 Effects of Insonification on Cell Viability

In addition to insonification-related cell detachment, effects on cell viability were also investigated. The percent of viable cells was determined using equation (3) whereby the sum of viable cells which remained attached and those that re-attached was divided by the initial cell count. The viable fraction 1 hour after insonification and 24 hours after the initial imaging are displayed in Figure 4a and Figure 4b, respectively. One hour after excitation, the 6-watt power setting at 6 joules had the highest percentage of viable cells (approximately 60%). The lowest viability belonged to the 9-watt power series at 45 joules, where only 4% of the cells were still viable. The 15-watt power series showed a consistently low survival rate regardless of the energy into the system (<20%).

The 6-watt power series had a significant difference between 6 joules and 48 joules ( $p=0.023$ ). The 9-watt power series had significant differences between 9 joules and 45 joules

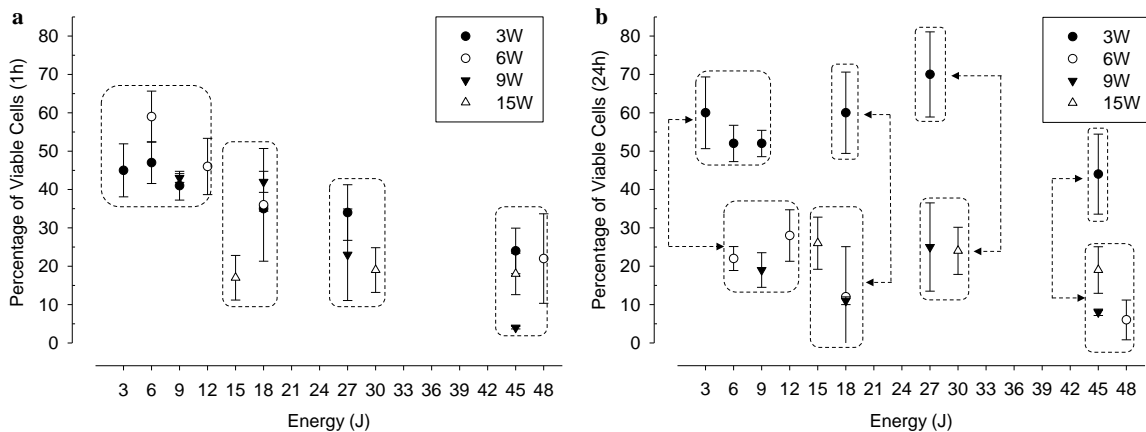


Figure 4. The percent of viable cells (a) 1 h or (b) 24 h after insonification at various power and energy levels. Data points grouped within dashed boxes show no significant differences among each other ( $p>0.05$ ). Groups of data with significant differences ( $p<0.05$ ) among different power series for similar energy ranges are indicated with dashed arrows.

( $p < 0.001$ ), and between 18 joules and 48 joules ( $p < 0.001$ ). There were no significant differences in the percent of viable cells between any energy levels in the 3-watt or 15-watt power series. Interestingly there were no significant differences among the different power series at similar energy levels. For example, exposing adhered cells to 3 watts 9 joules gives similar results as exposing them to 9 watts 9 joules. There were many significant differences between the 6 and 9-watt power series at different energy levels. This could indicate that initial viability is determined more by energy exposure than the power of the excitation.

At 24 hours after initial imaging, the 3-watt series retained the highest percent of viable cells over 24 hours. At all energy levels tested, the 3-watt series had significantly more cells remain viable than any other power input tested. For each power series, there were no significant differences in the percent of viable cells for all energy levels. However, there were significant differences between the percent of viable cells analyzed 1 hour after insonification and the percent of viable cells 24 hours after initial imaging. Overall, every point on the 3-watt series showed an increase in viable cells over 24 hours, indicating cell proliferation; however, only the samples exposed to an energy of 27 joules showed a statistically significant increase ( $p = 0.003$ ). Both the 6 and 9-watt power series trended towards a decrease in viable cells over 24 hours, with a few of the points significantly different. The 6-watt series at 6 joules showed a significant decrease ( $p = 0.026$ ). At 9 watts, both the 9 and 18 joule energy settings showed a significant decrease ( $p = 0.033$  and  $p = 0.003$  respectively). The 15-watt series had no significant increase or decrease in the percent of viable cells over 24 hours.

Overall, these findings showed that long term viability of cells after insonification depends on both power of the acoustic transducer and the energy into the system. It also demonstrated that the initial assessment of cell viability does not indicate long-term survival.

Cells exposed to 6 watts and 6 joules initially had the highest percent survive, but over 24 hours, these cells exhibited marked decreases in viability. Furthermore, while many cells initially survived detachment and were able to re-attach to a new surface, a majority of those (especially >3W) must have sustained damage since long-term viability was diminished ( $\geq 24$  h).

### 2.3.3 Effects of Distance from Source of Acoustic Excitation on Cell Attachment

Cell detachment was nearly uniform for insonification greater than 6 J; however, a distinct biphasic spatial distribution resulted in lower energy trials Figure 2e. The distribution comprised of overall higher cell survival and decreased cell detachment beyond a few millimeters from the source of excitation. A spherical pressure wave at the center of the dish, such as that generated by the sonicator microtip, would cause a radial gradient of insonification with an acoustic intensity that diminishes as it travels farther from the probe [49, 50].

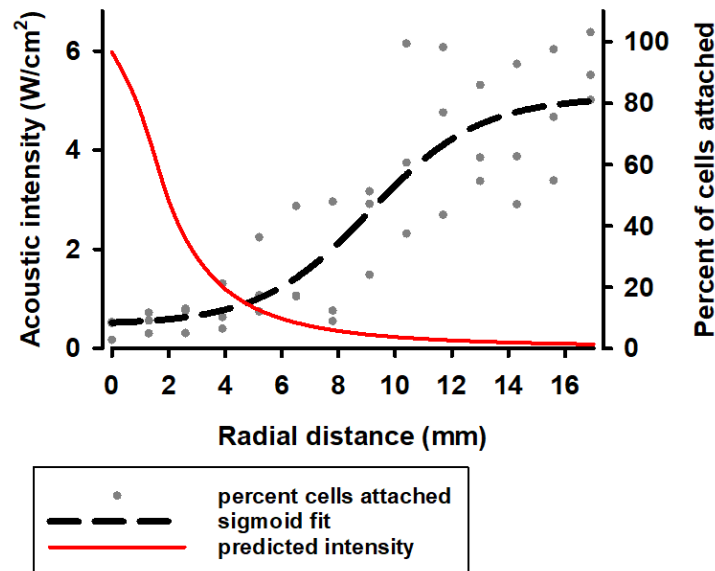


Figure 5. Relation between acoustic intensity and cell detachment after exposure to a power of 3 watts and energy of 3 joules (3W3J). Radial values are relative to the center of the dish, closest to the tip of the excitation source. A sigmoidal curve was fit to attached cells for 3 independent experiments.

In Figure 5, acoustic intensity for a spherical pressure wave emanating from the transducer tip, calculated using equation (4), is compared to the percent of cells remaining attached after insonification; both of these values are plotted from the center of the tissue culture dish to the outside edge in the radial direction. The power output from the transducer was divided by the cross-section area of the spherical pressure wave as it interacts with the surface of the dish to calculate the radial dependence of intensity. The calculated acoustic intensity was compared to the percent of cells remaining attached after exposure at corresponding radial locations. We observed that cell detachment had an inverse relationship with each cell's relative distance from the sonicator, and was directly related to the acoustic intensity incident on the surface.

Concerning established cell adhesion characterization methods, this result resembles the detachment trend in a radial flow assay where shear stress is inversely proportional to the radial position in the laminar flow [16]. Based on a sigmoidal fit of adherent cells after insonification with 3W for 1s, 50% of cells were removed at approximately 9.6 mm radially from the center, corresponding to a predicted  $0.26 \text{ W/cm}^2$ . Only the lowest power and energy settings available for these experiments had the range of intensity to allow the visualization of this distinct radial detachment profile. Correspondingly, this prospective threshold is exceeded at 14mm for 6W, 17mm for 9W and 22mm for 15 W. Since we were only able to measure out to 17mm from the center of the 35mm dishes used here, the mean adhesion strength of cells was presumably exceeded as far as the outer edge for all but the 3-watt series. Together, these results demonstrate the ability to fine-tune a range of acoustic excitation values which spatially control cell detachment while maintaining acceptable levels of cell viability. Further research into this technique is required to fully understand detachment profiles generated by the acoustic

transducer and to deduce a direct correlation to existing well-characterized detachment force models.

$$\text{Acoustic Intensity} = \frac{P_{\text{avg}}(W)}{4\pi r^2(\text{cm}^2)} \quad (4)$$

Finally, cellular damage and detachment due to cavitation effects are common concerns for sonication probes, such as the one used in this study. Cell damage caused by the shock of cavitation requires the microbubble to be within micrometers of the cell [51]. Cavitation microbubbles are initially formed at the tip of the probe[52]. Then the microbubbles will either implode, rise due to buoyancy forces, or be forced downwards towards the cells by the generated acoustic excitation or microstreams within the fluid [52]. In this study, the relatively large distance between the probe tip and the cell surface (2mm) minimized the probability of a microbubble coming within micrometers of a cell before imploding. It has been shown that as exposure time increases, cavitation microbubbles travel further down into the fluid medium before imploding; however, these times greatly exceed the length of exposure used within this study [52]. Therefore, it is unlikely that cavitation is the primary mechanism of acoustic-based cell detachment or destruction in this study. Instead, these results suggest that the excitation from the ultrasonic transducer is responsible for the mechanical manipulation and its impacts on cell adhesion distribution and viability observed here.

## 2.4 Conclusions

In summary, this study demonstrates that the power, energy, and intensity of an acoustic pressure wave have profound impacts on both cell attachment and viability. At similar energy values, higher power inputs corresponded to a higher percentage of cells detaching from the surface in shorter exposure times. However, as power and energy increased, long-term viability

of fibroblasts was compromised, with some samples retaining less than 10% of the original cells after 24 hours. This research also demonstrates that as the distance from the transducer increased, causing the relative acoustic intensity to decrease, there was a corresponding decrease in detachment of cells. Acoustic transducers generating pN scale forces have previously been used to trap or move suspended cells and high-intensity acoustic transducers are commonly used for cell destruction; these results indicate that the application of intermediate levels of excitation from acoustic transducers may be useful in manipulating or measuring the adhesion strength of stably adhered cells, or even in selectively patterning cell populations. Further investigation is warranted to determine the mechanism by which insonification negatively impacts viability such that manipulation can be fine-tuned, and stimulation protocols can be developed. Additionally, native tissue consists of multiple different cell types; thus, cells other than fibroblasts should also be investigated to determine how similar ranges of acoustic excitation affect different types of cells.

## Chapter 3: Manipulation and Patterning of Cells using Acoustic Forces

### 3.1 Background

Vibration is defined as the oscillation of particles within an elastic body or fluid about an equilibrium point. This natural mechanical phenomenon affects every physical system in the universe as long as that system has mass and stiffness. The relationship between a system's mass and stiffness defines its natural frequency, or the frequency a system vibrates at in the absence of outside forces. Resonance occurs when a system is driven at its natural frequency; producing large amplitude oscillations which often cause catastrophic failure.

In 1787 German physicist Ernst Chladni published a technique which allowed for the visualization of various modes of vibration on a rigid surface. This was accomplished by drawing a bow over a flat metal plate until the plate reached resonance, effectively creating a standing wave. Sand on the surface of the plate would move towards locations of zero amplitude, known as nodal points, and away from points of maximum amplitude, known as antinodal points.

Michael Faraday, fascinated by Chladni's work, discovered what is now known as Faraday instability back in 1831 [53]. Faraday instability is the terminology used to describe nonlinear standing waves which appear in liquids enclosed within a vibrating container. Similar to Chladni patterns, Faraday waves can take many forms depending on multiple factors including, but not limited to, frequency and amplitude of oscillation, depth of the liquid, and material properties of both the liquid and its container.



Recently, scientists have begun taking advantage of Faraday waves to assemble biological materials such as cells, cell spheroids, and cell-seeded microcarrier beads.

This central theme of this research focuses on the manipulation and patterning of cells in a common tissue culture dish using vibrational and acoustic forces. Preliminary work has proven the importance of computer modeling for accurate prediction of the parameters required to achieve specific patterns. Insights gained from the previous section aids in the development of these computer models and experimental data is used to verify accuracy. Successful cell patterning is performed and both long term cell viability and pattern retention over time are investigated; ensuring this new method of cellular manipulation is practical.

### **3.2 Computer Modeling and Experimental Validation**

Physical systems theoretically have an infinite number of natural frequencies; however, only a limited number of specific frequencies will generate a desired pattern. Thus, experimentally identifying the parameters to generate specific patterns is impractical. This type of problem can be resolved using computer modeling to predict potential useful frequencies which are verified experimentally. Both SolidWorks and Ansys were used to find natural frequencies of a 100mm polystyrene tissue culture dish and results from each were compared to ensure accuracy.

Table 1 shows the first 10 modes and corresponding frequency in Hz for the same tissue culture dish analyzed in SolidWorks and Ansys. Figure 6 illustrates results of SolidWorks simulation results compared with images from sand inside a tissue culture dish being stimulated at the given frequency. Initially the sand clung to the tissue culture dish resulting in uneven pattern formation. This was remedied by rubbing the dish with a simple dryer sheet to remove any static electricity, results shown in Figure 6.

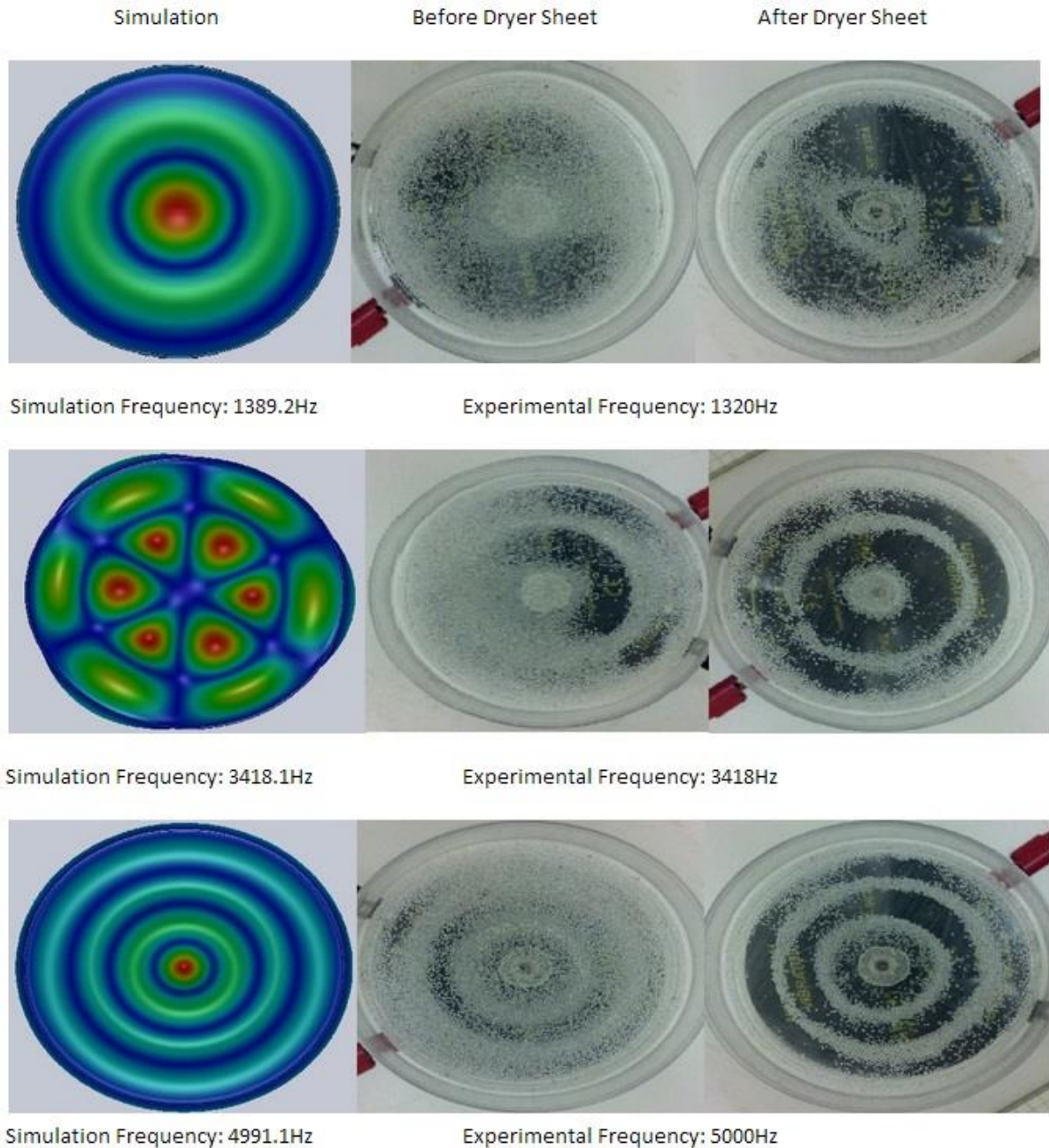


Figure 6 SolidWorks modal frequency simulation results compared to experimental modal frequencies.

Modeling natural frequencies and mode shapes in air is relatively simple; however, this does not accurately represent the environment of a mammalian cell in culture. Mammalian cells die rapidly in air and require medium in culture to survive. This medium is mostly water with dissolved minerals, proteins, growth factors, and antibiotics. Knowing this, the medium must be

accounted for in order to generate an accurate model of the experiment. The liquid will add mass, dampen resulting vibrations, and introduce streaming effects which were not a factor previously. Adding mass to the system and dampening vibrations dramatically lowers the frequency these mode shapes take place.

### **3.3 Methods and Experimental Setup**

#### **3.3.1 Cell Culture and Reagents**

NIH3T3 murine embryonic fibroblasts (CRL-1658, ATCC) were cultured in complete growth medium (CGM) containing 10% new born calf serum and 1% penicillin-streptomycin in Dulbecco's modified Eagle's medium. Cells were passaged every three days using 0.25% trypsin-EDTA and used between passages 5 and 20. Cell culture reagents were purchased from Invitrogen unless otherwise noted.

CellTracker Green CMFDA was diluted to a working solution of 20  $\mu\text{M}$  in DMEM following the protocol from Thermo Fisher [54]. Culture media was removed from adhered fibroblasts and the dish was rinsed with DPBS (++) before adding 2ml of the CMFDA solution. Cells were then incubated at 75% relative humidity, 5%  $\text{CO}_2$  and 37°C for 45 minutes.

Calcein AM Green was diluted to a working solution of 2  $\mu\text{M}$  in DMEM following the protocol from Thermo Fisher [55]. Culture media was removed from adhered fibroblasts and the dish was rinsed with DPBS (++) before adding 2ml of the calcein AM solution. Cells were then incubated at 75% relative humidity, 5%  $\text{CO}_2$  and 37°C for 45 minutes.

Cell manipulation experiments were performed on NIH3T3 fibroblasts stained with either CellTracker Green CMFDA, CellTracker Orange CMTMR, or Green Calcein AM to visually verify pattern formation. CMFDA and CMTMR were chosen when imaging the cells over multiple days as they remain fluorescent for over 3 days and transfer to daughter cells when

cell division occurs [54]. CMTMR was chosen to differentiate between cell patterns when multiple pattern experiments were performed. Calcein AM was chosen when assessing cell viability and when short term fluorescence was required as fluorescence from calcein AM is only retained in live cells and quickly dissipates if the cell's membrane is compromised [40, 41].

### 3.3.2 Cell Manipulation

A mechanical vibrator (Pasco Scientific SF-9324), controlled using a 12MHz DDS sweep function generator (BK Precision model 4013DDS), was used to manipulate cells in suspension. In order to manipulate cells using a mechanical vibrator, a sterile tissue culture dish was affixed with a banana plug which fit into the vibrator. A guide was drawn up in SolidWorks and 3D printed to ensure accurate placement of the banana plug in the center of each tissue culture dish. Originally the banana plug was directly adhered to the dish using cyanoacrylate (super glue); however, this posed an issue with automated fluorescent microscopy imaging as the banana plug prevented the objective from getting within working distance of the dish. This was remedied by sandwiching a small glass coverslip between the banana plug and the dish. After 3 hours in the incubator, the glue between the banana plug and the glass cover slip weakened enough to be easily removed by hand without damaging the tissue culture dish.

80% confluent dishes containing adhered fibroblasts were stained using one of the protocols above, rinsed of any remaining staining solution using Dulbecco's phosphate buffered saline without calcium or magnesium (DPBS --), and incubated at 75% relative humidity, 5% CO<sub>2</sub> and 37°C with 2ml of 0.25% trypsin-EDTA for 5 minutes. 8ml of fresh CGM was then added to the dish and gently pipetted 20 times to dislodge any remaining adhered cells. The suspended cell solution was then moved to a 15ml conical tube and spun down in a centrifuge at

300 rcf for 5 minutes to form a pellet. The media was then aspirated off of the top and the pellet was suspended in 5ml of fresh CGM to remove any remaining trypsin-EDTA.

The 5ml suspended cell solution was then added to a tissue culture dish with a banana plug attached to its center and moved to a mechanical vibrator. Here the cells were exposed to a vibration at a specified frequency and amplitude for 1 minute. After the minute was up the mechanical vibrator was turned off and the dish was left undisturbed for 1 hour to allow for cell adhesion [38]. After 1 hour the dish was carefully moved to the incubator at 75% relative humidity, 5% CO<sub>2</sub> and 37°C for 3 additional hours. Once 4 total hours were up the media was gently aspirated off and 10ml of fresh CGM was added. Pattern formation and fidelity was then analyzed using automated fluorescent microscopy.

### 3.3.3 Automated Fluorescent Microscopy Analyses

Samples were imaged and pattern fidelity analyses were performed using an Eclipse Ti-U (Nikon Instruments) inverted microscope equipped with a CCD camera (CoolSNAP HQ2 Photometrics) and appropriate fluorescent filter sets. Automated fluorescence microscopy, controlled by NIS-Elements software (version 4.20, Nikon Instruments), was used to capture and stitch together 41x10 images for each sample on each day. This automation used a computer controlled stage, in conjunction with the microscope setup described above, to capture fluorescent images at 410 different locations, 10 columns of 41 images, traveling radially on each dish for a total analysed area of 439 mm<sup>2</sup> (8% of total dish area). The images were saved and stitched together with a 5% overlap, resulting in a final image which was 12669 pixels wide by 38480 pixels tall, or 10895.34 μm wide by 33092.8 μm tall. This final image covered an area of 360.5mm<sup>2</sup> (6.5% of total dish area). Fluorescent intensity data over the radial direction, normalized to the background fluorescence, was recorded for each sample.

### 3.3.4 Macro Fluorescent Image Analyses

Pattern formation and fidelity was also confirmed using macro images of the dish. Fluorescence was expressed using blue 470nm (Thorlabs LIU103) or green 525nm (Thorlabs LIU525A) LEDs with appropriate glass filters 495nm LongPass (Thorlabs FGL495S) or 590nm LongPass (Thorlabs FGL590S). A Nikon d3200 digital SLR equipped with magnification lenses ranging from 1x-10x was used to capture images corresponding to  $t=0$  (before excitation), 1 minute (after excitation), 4 hours, 24 hours, and 48 hours. These images were used to empirically confirm initial pattern formation and retention over time.

## 3.4 Results and Discussion

### 3.4.1 Simulation Validation

Previous experimental work has shown sand particles can be patterned inside a common tissue culture dish. This was accomplished by rigidly fixing the dish to a simple mechanical shaker and controlling the amplitude and frequency of actuation with a function generator. Initial modal analysis results of a normal 100 mm tissue culture dish was performed using SolidWorks and Ansys to ensure accuracy of the model, briefly displayed in Table 3.4.1. These results match up with the experimental results in air as seen in Figure 6.

The next step was to see if particle size impacted the particle's movement to nodal locations. Similarly, polystyrene microspheres were patterned at the same frequencies; again showing excellent results when compared to the simulations; indicating that the size of the particles being patterned does not play a large role in pattern formation in air.

Since mammalian cells must be suspended in liquid the obvious next step was to add liquid to the simulation and verify via experimentation. However, addition of a liquid to the

simulation renders modal analysis moot since liquids do not have a Young's Modulus. Future computer modelling of the system must be performed using vibrational or acoustic forces and solid-fluid interactions.

Table 1 SolidWorks vs Ansys modal simulation results for a 100mm polystyrene tissue culture dish

Mode	SolidWorks Frequency [Hz]	Ansys Frequency [Hz]
1	720.05	727.52
2	720.12	727.75
3	736.1	740.29
4	736.14	740.72
5	950.43	959.43
6	950.44	959.55
7	1109.1	1114.5
8	1109.1	1114.8
9	1210.7	1221.1
10	1210.7	1221.4

Introducing a liquid medium makes the system more complex. Liquids, such as water or CGM, introduce mass, damping, and fluid forces on particles becomes a factor. Additional mass is easy to model and simply shifts the modal frequencies down such that the same modes appear at lower frequencies. However, damping and fluid forces on particles must also be taken into consideration. Liquids move and shift with the vibration; this happens in air as well but the overall fluid dynamic effects on the particles are significantly lower than the fluid dynamic effects of particles suspended in a liquid.

A brief experiment, example results shown in Figure 7, was performed with 10 $\mu$ m diameter polystyrene spheres suspended in 5ml of DI H<sub>2</sub>O. The dish was vibrated at all of the frequencies previously explored but no movement of the microspheres was recorded. The frequency was then dramatically lowered in order to find the mode shapes experimentally. The dish was swept through a range of frequencies and still no pattern formed. However, at certain frequencies the flow of the water became turbulent which suggests the dish was being vibrated near one of its modal frequencies. The amplitude of the vibration was then adjusted. Eventually this led to the microspheres moving within the dish to the nodal locations and successful pattern formation. This finding further suggests that fluid forces play a pivotal role when the particles are suspended in liquid rather than in air.

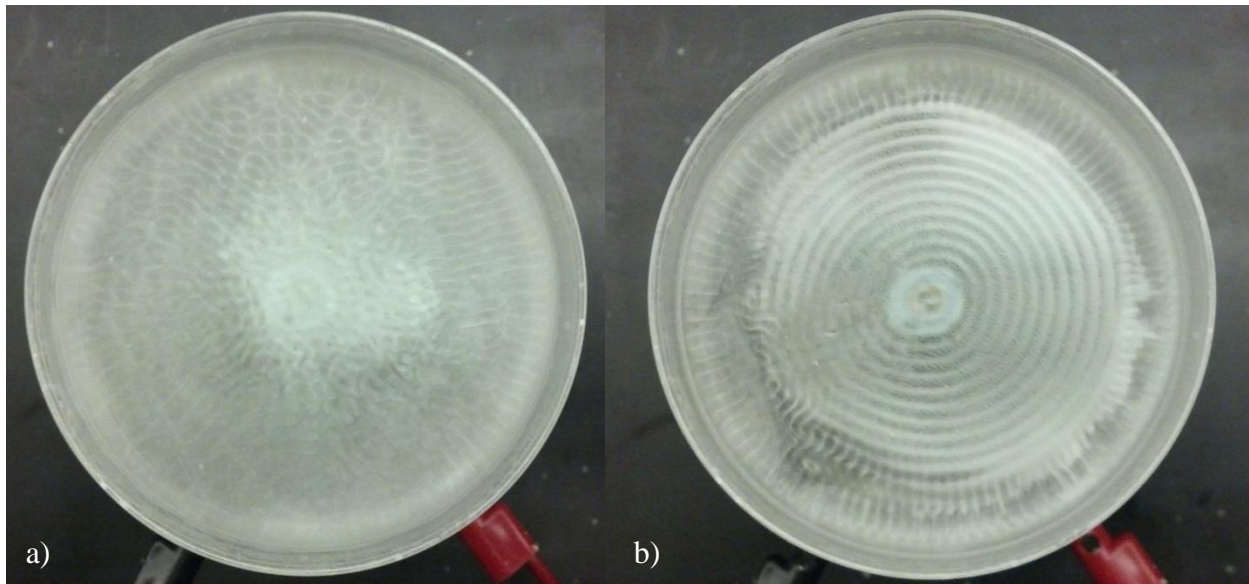


Figure 7 10 $\mu$ m polystyrene spheres in 5ml of DI H<sub>2</sub>O at 75Hz. a) full amplitude b) half amplitude



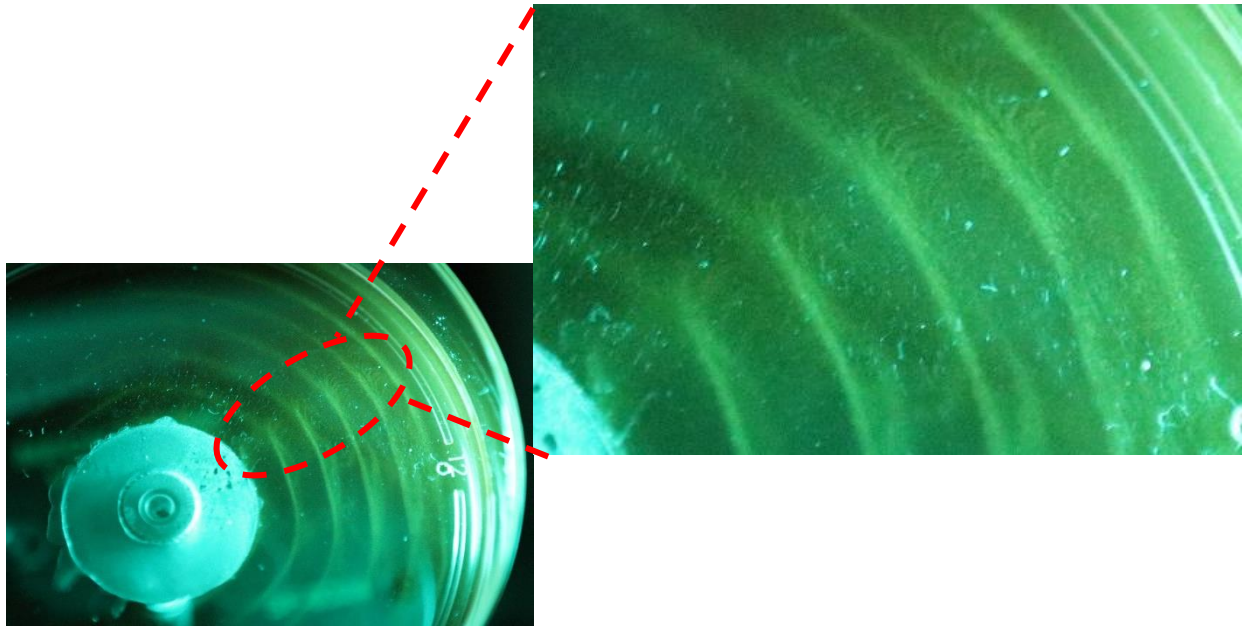


Figure 8 Macro image of green fluorescent NIH3T3 fibroblasts during vibrational patterning at 40Hz. Cells are moving in streamlines from the inner nodes towards the outer nodes.

### 3.4.2 Cell Pattern Characterization using Macro Images

Suspended NIH3T3 fibroblasts were subjected to one of two frequencies, 40Hz or 75Hz, for 1 minute. Each sample was run in triplicate to ensure the accuracy of the data collected.

Macro images were taken in order to empirically verify pattern formation. Figure 8 was captured during vibrational patterning. The lines are made up of NIH3T3 fibroblasts fluorescing green.

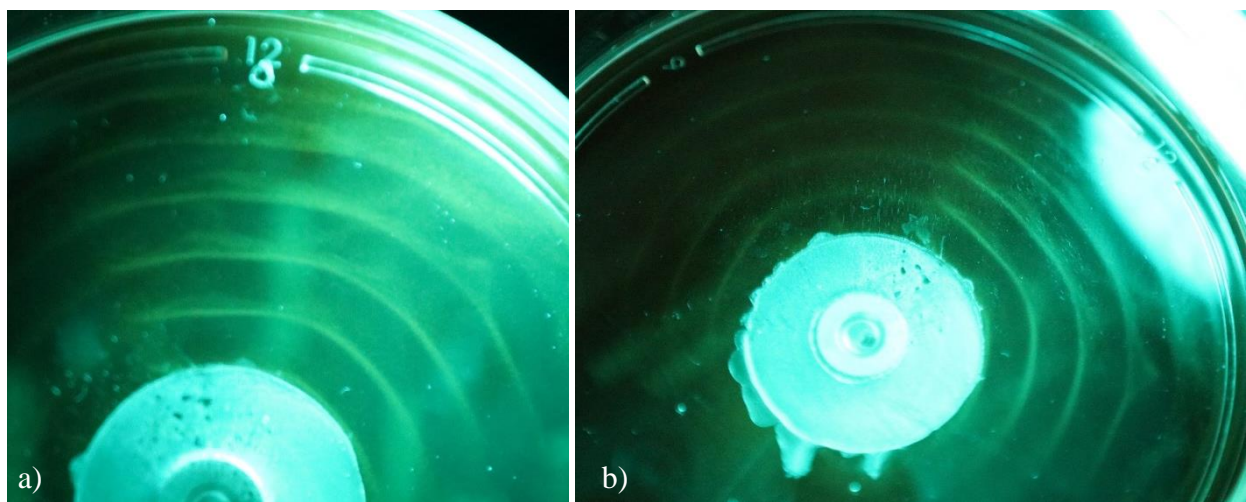


Figure 9 Macro image of NIH3T3 fibroblasts after patterning at 40Hz. a) immediately after vibrational force ends cells no longer streamlining between nodes and starting to settle into nodal locations. b) A 1 hour after vibrational force ends

This image shows that the cells are being forced towards nodal locations on the dish. The zoomed in portion of the figure shows the cells seem to be moving in streamlines.

Figure 9a shows the same dish immediately after the vibrational force was concluded. A majority of the cells have been forced to the nodes. Some cells are still suspended in the fluid column and will float down to the surface of the dish. Figure 9b was taken 1 hour after the vibrational force was concluded to allow precipitation of the suspended cells and adhesion to the surface. This shows that a majority of the cells in the dish have been successfully patterned and 1 hour after stimulation the cells remain in the nodal locations.

Pattern reproducibility was also assessed using macro images. Figure 10 shows another dish that was patterned at 40Hz. Comparing this with Figure 9, it is evident that a 40Hz vibration forces the cells into a pattern with 6 defined bands and very few cells in between.

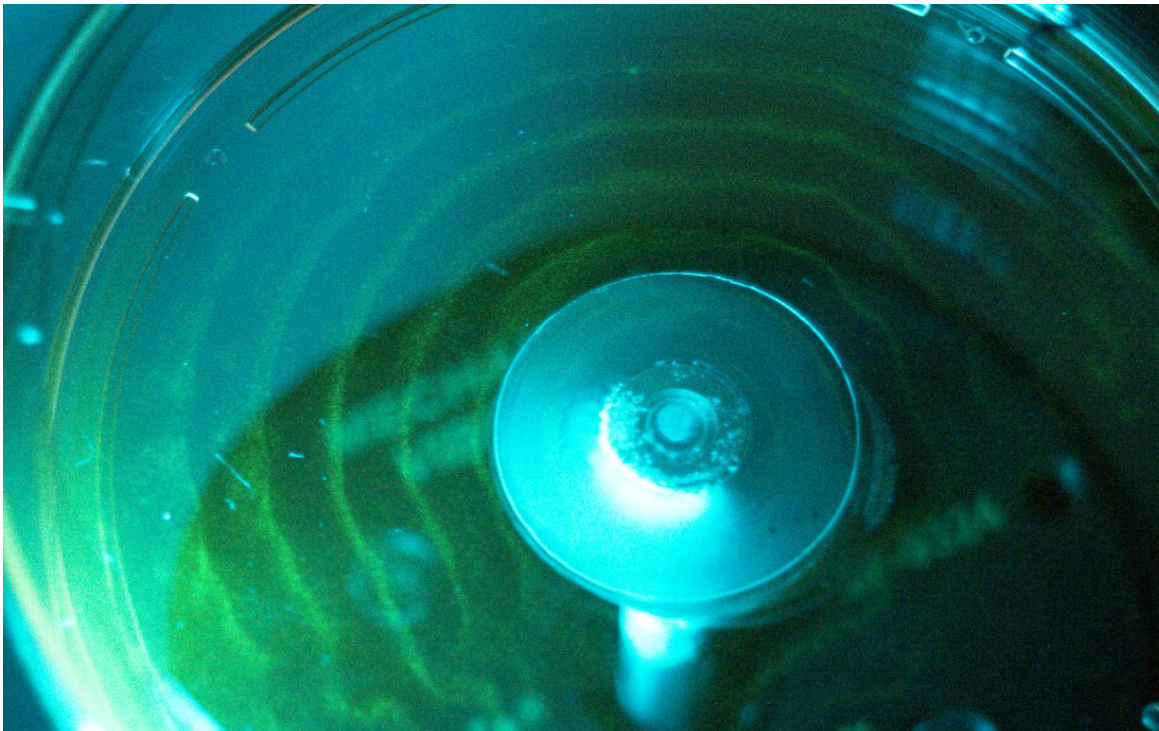


Figure 10 Macro image of NIH3T3 fibroblasts after patterning at 40Hz. This shows an almost completely symmetric pattern formation over the majority of the dish

Pattern symmetry was also assessed using macro images. While each pattern could be reproduced reliably, not all of the patterns turned out symmetric. Figure 10 is one example with around three-quarters of the dish was successfully patterned. Partial patterning was a consistent problem during this study. The single point of contact between the tissue culture dish and the mechanical vibrator was most likely the cause of these partial patterns. One point of contact leaves multiple degrees of freedom where the dish could move. In some trials the vibration caused the banana plug-dish assembly to lean to one side, creating a non-symmetric pattern. In order to obtain a perfectly symmetric pattern, the dish would have to remain perfectly level both during excitation and until the cells attached to the surface.

As previously stated, amplitude of vibration also became a factor once liquid was introduced. Figure 11 shows fibroblasts, fluorescing green, during excitation, 40Hz, at an

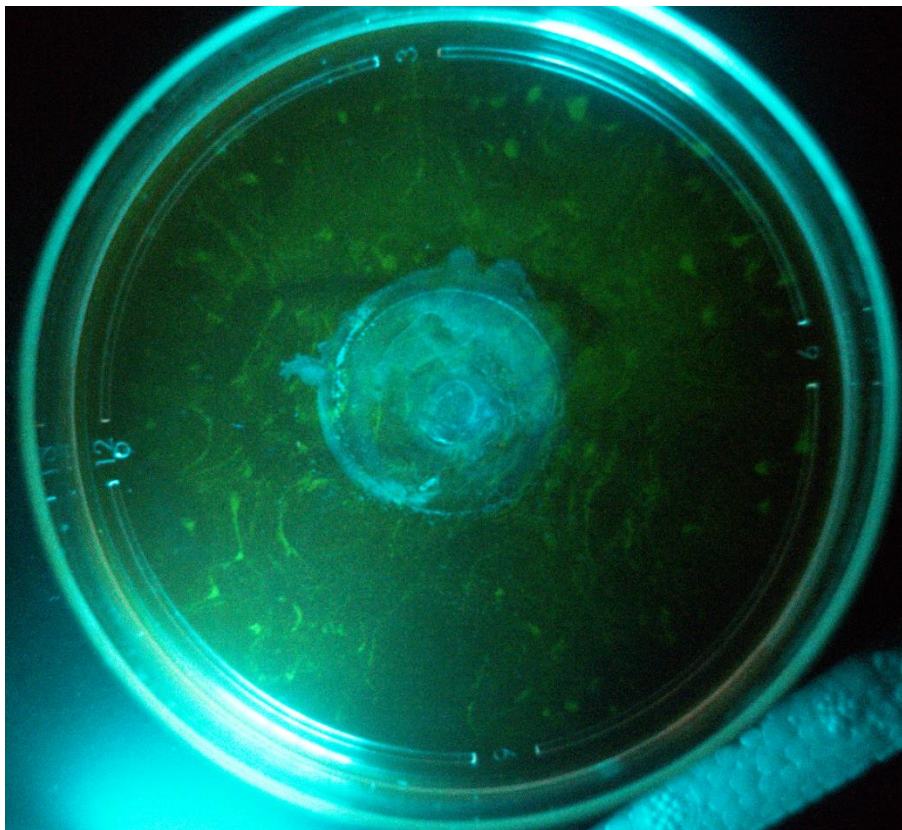


Figure 11 Macro image of NIH3T3 fibroblasts at 40 Hz with increased amplitude. Cells cannot be forced to nodal locations due to turbulent flow of the media

increased amplitude than what was found adequate for patterning. The increased amplitude causes turbulence in the media which in turn overrides the vibrational force placed on the cell.

With this additional force, the cells are not able to settle at nodal locations.

### 3.4.3 Cell Pattern Characterization using Automated Fluorescent Microscopy

Cell pattern formation was characterized using automated fluorescent microscopy.

Representative images, Figure 12 and Figure 13 empirically demonstrate pattern formation and retention over time. These images are composed of 10x41 individual fluorescent images stitched together with a 5% overlap.

Figure 12 represents results taken from a pattern formed using a frequency of 40Hz while Figure 13 represents results taken from a pattern formed using a frequency of 75Hz. During excitation, suspended cells were forced into nodal locations and clustered together to form defined bands of cells. The number of bands correlates to the frequency of excitation and can be seen in these images; 5 bands were formed at 40Hz and 8 bands were formed at 75Hz. The distance between each band appears to be constant, with the exception of the furthest two bands created from excitation at 40Hz. This could be due to a reflection of the vibrational waves at the wall of the tissue culture dish creating an additional node but further investigation is needed to verify this hypothesis. The bands created from excitation at 75Hz all appear equidistant from each other.

It should be noted that while a majority of cells were successfully patterned during excitation, these images show that some cells attached outside of nodal locations. This was expected for two reasons. First, cells were suspended in CGM during excitation. Forces caused by the vibration of the culture dish vary throughout the height of the fluid column; therefore, cells floating near the surface of the CGM will experience different forces than cells floating

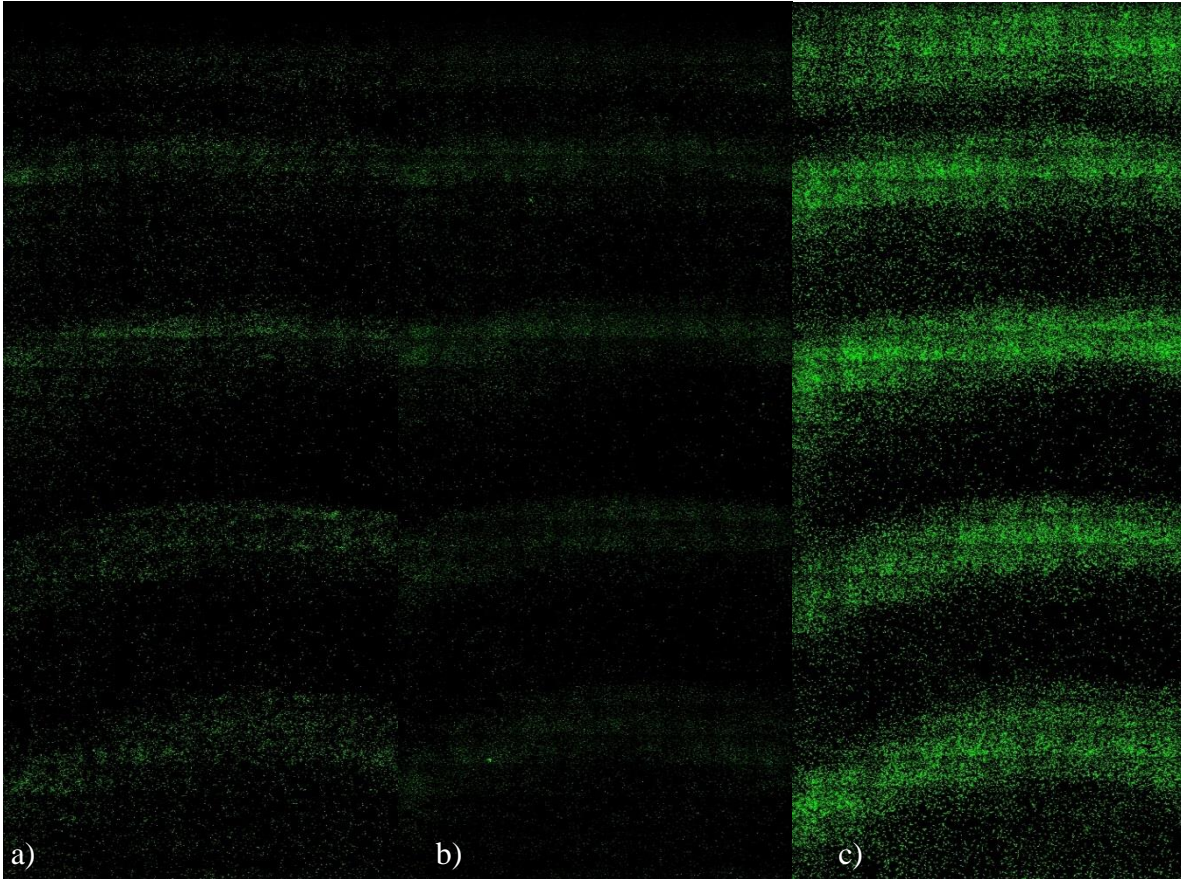


Figure 12 Representative image of NIH3T3 Fibroblasts patterned at 40Hz. a) 4 hours after patterning. b) 24 hours after patterning. c) 48 hours after patterning

near the surface of the dish. This difference in force could cause some cells to remain suspended over non nodal locations, eventually sinking down and attaching after excitation is concluded. Second, cells were allowed to adhere to the surface for 1 hour after excitation, enough time to develop around 40% of their normal adhesion strength [42]. The media was then aspirated off and new CGM was added to the dish. It is possible that some of the attached cells were detached and carried to a different location by the flow of new media.

Figure 12 and Figure 13 also show that the pattern formed during excitation is mostly retained even after 48 hours under normal culture conditions. Parts b) and c) of each figure, 24 and 48 hours after patterning, display an increase in both pattern band width and number of cells in between bands when compared to the initial pattern shown in a) of each figure. This is most

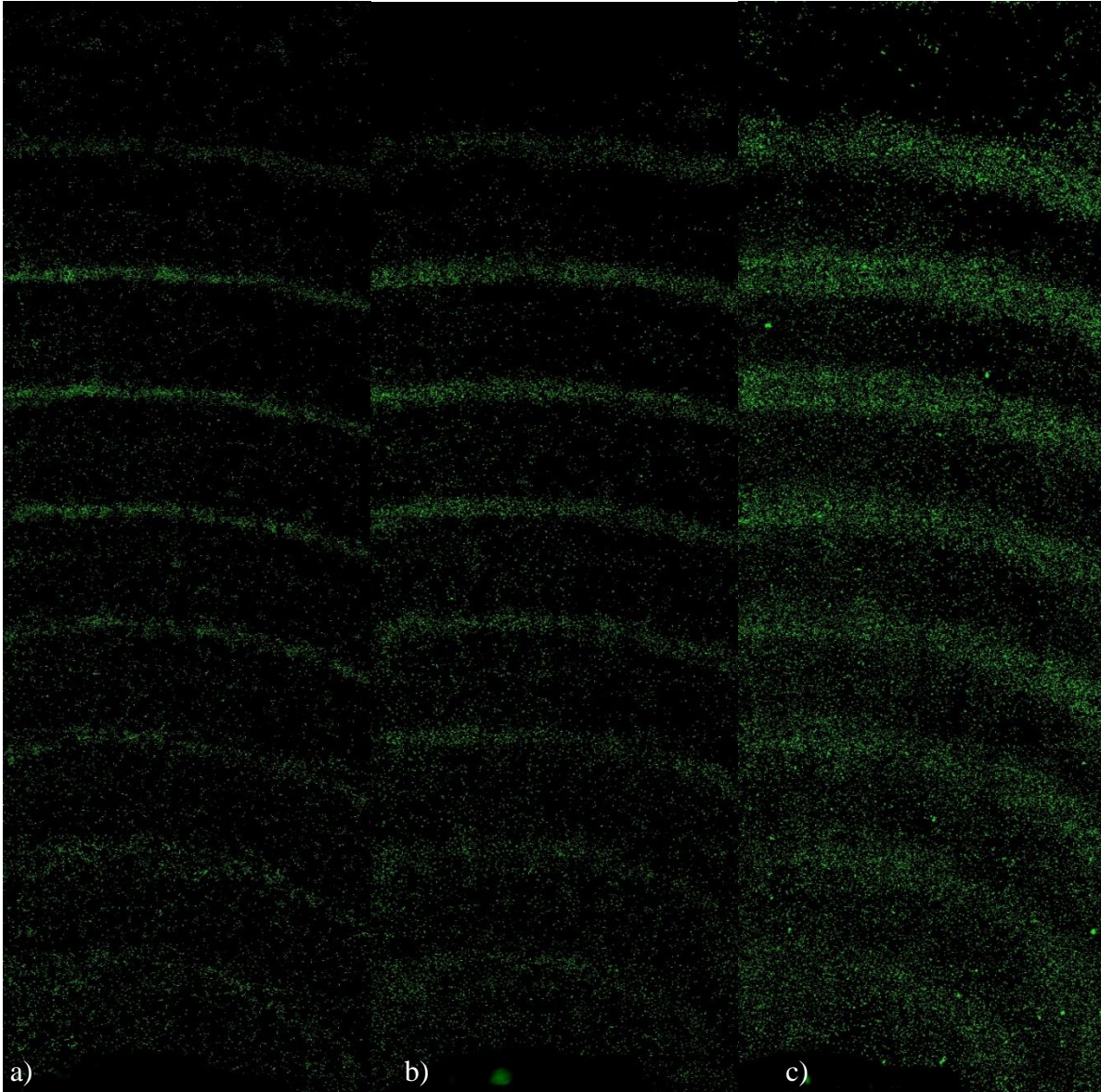


Figure 13 Representative image of NIH3T3 Fibroblasts patterned at 75Hz. a) 4 hours after patterning. b) 24 hours after patterning. c) 48 hours after patterning

likely caused by normal fibroblast migration and proliferation. Previous studies in wound healing show that, under normal conditions, NIH3T3 fibroblasts which are in contact with one another begin to migrate to locations void of fibroblasts within 24 hours. Therefore, the increase in pattern band width over time can be partially contributed to the clusters of fibroblasts migrating away from each other and into less dense areas outside of the original pattern. Additionally, parts b) and c) of each figure appear to have a higher number of cells contained within the same

imaging area, with c) containing the largest number of cells. Normal, healthy NIH3T3 fibroblasts have a doubling time of 20 hours so in both figures b) should have double the amount of cells that were in a) and c) should have four times as many as a). While the effects on long term cell proliferation was not explicitly investigated, data gathered from these images suggests that there are few, if any, harmful effects. Overall, these figures show that while some migration does occur and the cells seem to proliferate normally, the overall pattern is retained up to 48 hours after initial patterning.

The length between each band of cells was calculated by measuring from the midpoint of each band to the bottom of each image as shown in Figure 14. Patterns created were circular, so measurements were taken at five different locations to ensure accuracy of the distance between each band. The data is shown in Table 2-7; respective averages and standard deviations are plotted on Figure 15.

Patterns created using a frequency of 40Hz displayed 5 bands of cells clustered together. Distance between the first four bands on days 1, 2, and 3 averaged  $4777 \pm 56.1\mu\text{m}$ . The distance between bands 4 and 5 averaged  $5142.3 \pm 55.6\mu\text{m}$  for the first two days and  $4972.1 \pm 34.2\mu\text{m}$  on day 3. This discrepancy between the centers of cell bands 1-4 and 4-5 is not significant, therefore it is still a question as to why the 5<sup>th</sup> band is seemingly much closer to the 4<sup>th</sup> than the other bands.

Patterns created using a frequency of 75Hz displayed extremely consistent distances between the center of each band of cells. Days 1 and 2 had an average distance of  $3315.3 \pm 224.5\mu\text{m}$  and  $3316 \pm 235.4\mu\text{m}$  respectively while Day 3 had an average distance of  $3287.1 \pm 164.5\mu\text{m}$ . While these distances are not significantly different, it does show the center of the band of cells shifts slightly after 48 hours.

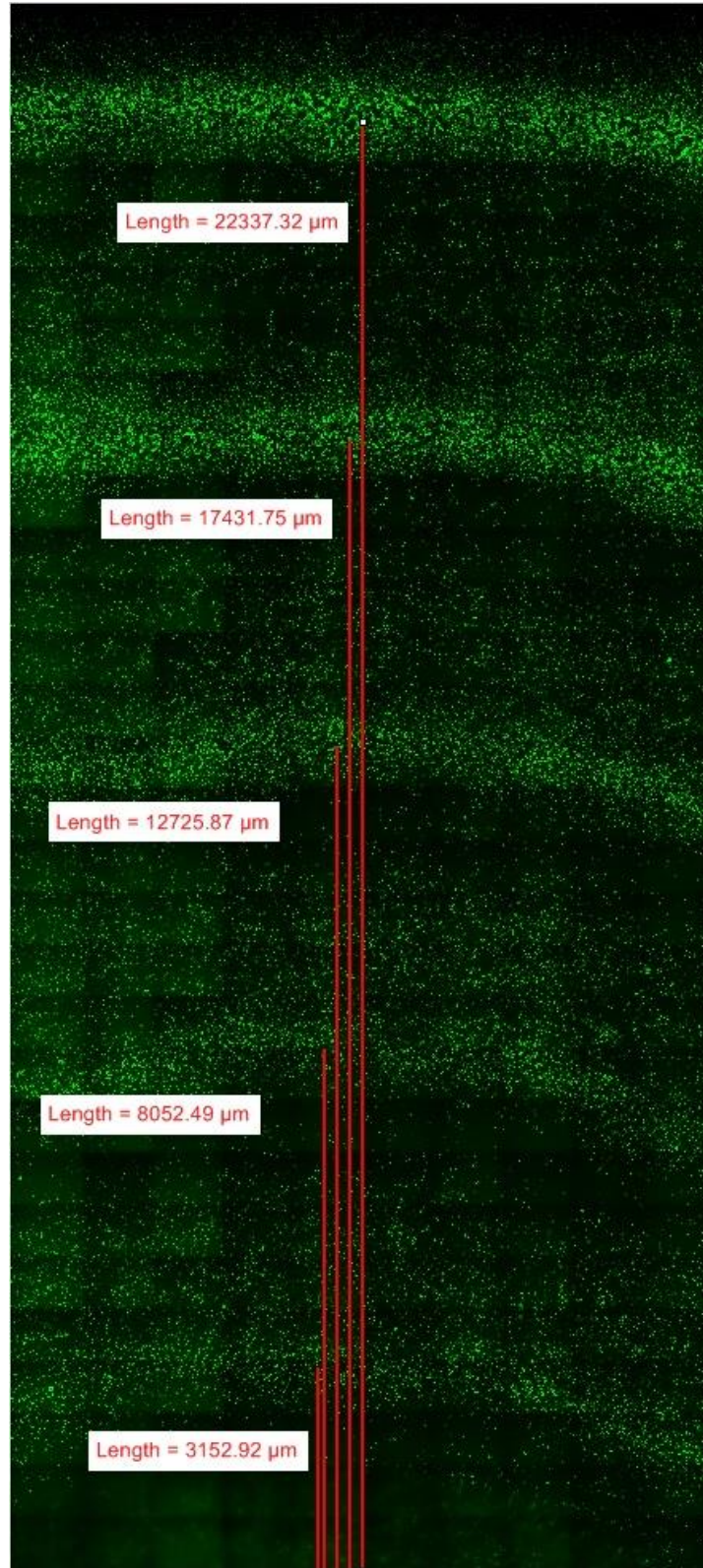


Figure 14 Representative image of distance measurements



Table 2 Longitudinal measurements of the distance between the center of the bands of cells for 40Hz on Day 1

Cell Cluster	Distance between bands of cells ( $\mu\text{m}$ )				
First to Second	4689.62	4597.12	4874.65	5090.08	4929.99
Second to Third	4875.36	4566.76	4659.3	4659.31	5091
Third to Fourth	4905	4874.16	4843.32	4843.31	4936.11
Fourth to Fifth	5275.79	5121.53	4967.27	4936.43	5214.11

Table 3 Longitudinal measurements of the distance between the center of the bands of cells for 40Hz on Day 2

Cell Cluster	Distance between bands of cells ( $\mu\text{m}$ )				
First to Second	4508.75	4601.3	4976.84	5066.12	5126.54
Second to Third	4350.28	4597.23	4442.45	4746.45	4871.79
Third to Fourth	4843.84	5121.39	4886	4832.51	4796.43
Fourth to Fifth	5275.85	5244.99	5141.13	5051.57	5194.78

Table 4 Longitudinal measurements of the distance between the center of the bands of cells for 40Hz on Day 3

Cell Cluster	Distance between bands of cells ( $\mu\text{m}$ )				
First to Second	5361.09	5392.11	4953.06	5240.84	4761.36
Second to Third	4308.28	4018.54	4254.33	3998.65	4637.77
Third to Fourth	4882.55	4978.28	4754.55	4850.54	4371.1
Fourth to Fifth	5074.55	5234.11	5010.39	4754.67	4786.71

Table 5 Longitudinal measurements of the distance between the center of the bands of cells for 75Hz on Day 1

Cell Cluster	Distance between bands of cells ( $\mu\text{m}$ )				
First to Second	3661.34	3040.8	2877.15	2808.96	3988.63
Second to Third	3061.36	3336.25	3461.96	3506.46	3145.05
Third to Fourth	3441.02	3306.84	3177.21	3155.44	3291.85
Fourth to Fifth	3297.52	3196.74	3302.8	3209.8	3427.98
Fifth to Sixth	3275.02	3264.8	3264.79	3306.63	3346.39
Sixth to Seventh	3281.84	3186.18	3349.29	3378.01	3399.49
Seventh to Eighth	3209.29	3347.58	3575.42	3405.69	3161.21

Table 6 Longitudinal measurements of the distance between the center of the bands of cells for 75Hz on Day 2

Cell Cluster	Distance between bands of cells ( $\mu\text{m}$ )				
First to Second	3851.42	3210	2913.98	3209.4	4055.31
Second to Third	3128.19	3251.97	3083.23	3421.08	2998.13
Third to Fourth	3434.76	3293.57	3378.2	2913.72	3589.17
Fourth to Fifth	3253.45	3251.64	3336.75	3463.13	3124.94
Fifth to Sixth	3276.62	3209.93	3294.67	3421.24	3462.98
Sixth to Seventh	3133.14	3209.25	3294.8	3294.3	3462.98
Seventh to Eighth	3225.57	3336.39	3418.99	3335.37	2956.2

Table 7 Longitudinal measurements of the distance between the center of the bands of cells for 75Hz on Day 3

Cell Cluster	Distance between bands of cells in $\mu\text{m}$				
First to Second	3547.97	3031.72	3294.18	3417.37	3209.6
Second to Third	3209.17	3008.04	3209.82	2913.68	3378.53
Third to Fourth	3378.5	3300.11	3378.25	3506.05	3716.44
Fourth to Fifth	3167.36	3325.09	3082.9	3250.44	3294.05
Fifth to Sixth	3378.87	3138.64	3336.28	3336.48	3251.82
Sixth to Seventh	3040.31	3220.59	3167.48	3251.59	3590.25
Seventh to Eighth	3294.16	3210.09	3420.73	3462.97	3462.38

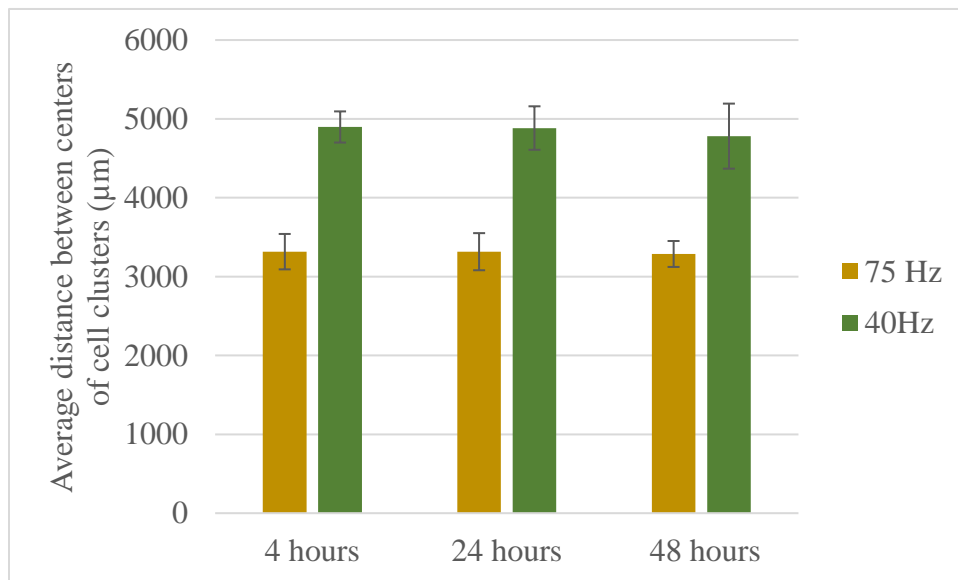


Figure 15 Average distances and standard deviations between bands of cells over time

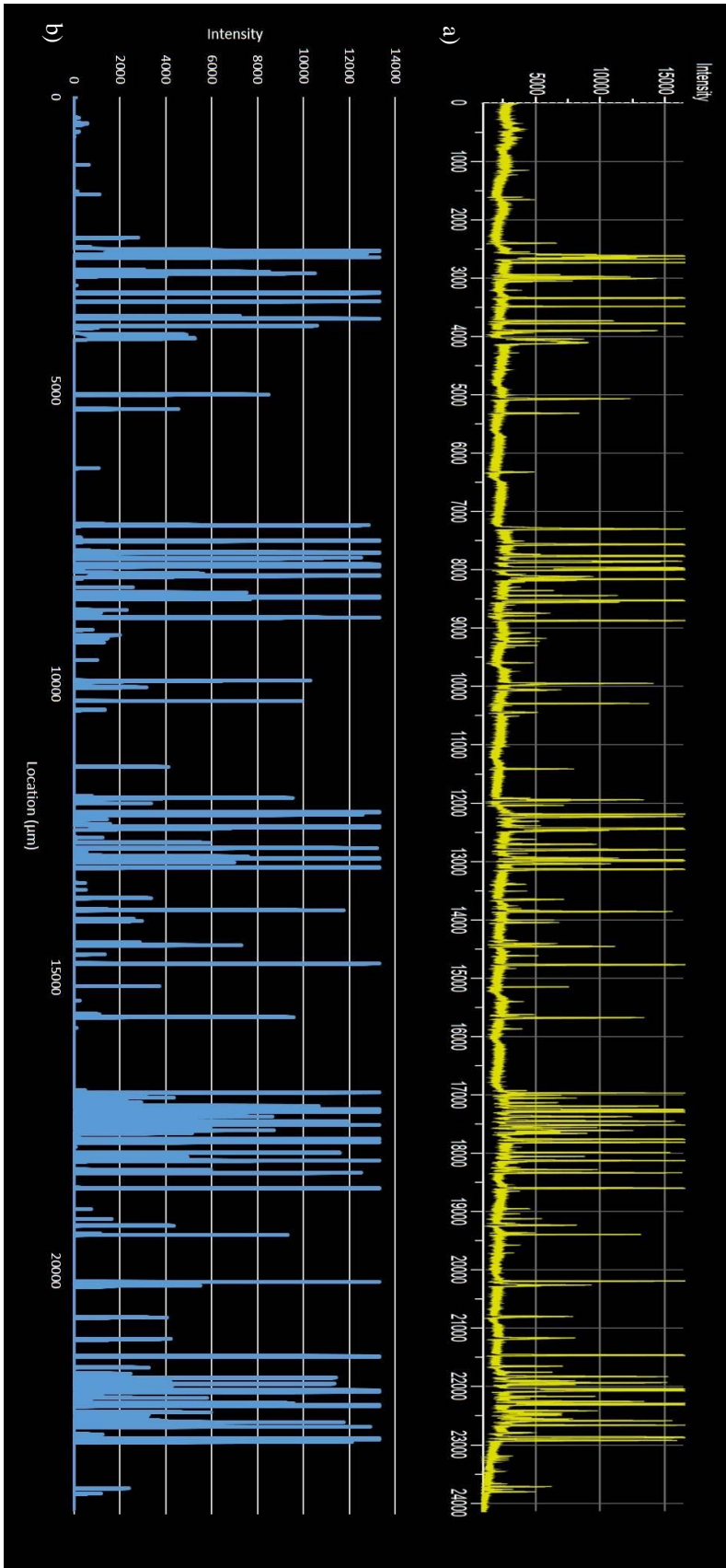


Figure 1-6 Representative fluorescent intensity vs location for 40Hz. a) Data before subtracting background fluorescence. b) Data after subtracting background fluorescence.

Fluorescent intensity over location was also analyzed, as shown in the representative image Figure 16. High fluorescent intensity directly correlates to locations where the green fluorescence stain, CMFDA, is expressed within the cells. Low fluorescent intensity correlates to locations where there are no cells, only background fluorescence is captured. This data was gathered in a 1 pixel wide measurement along the length of the stitched images. A total of five, 1 pixel wide measurements were taken for each sample on each day of analysis. The line measurements analyzed were located at: (1) left side of the first column of images, (2) 3<sup>rd</sup> column from the left, (3) 5<sup>th</sup> column from the left nearest to center of stitched image, (4) 3<sup>rd</sup> column from the right, and (5) right side of the final column. It is important to note that, due to the 1 pixel wide measurements, the data contains intensity spikes between the patterned bands of cells. These spikes are most likely due to individual cells on the culture dish which were not patterned properly and happened to be within the field analyzed. Figure 16a) represents the data gathered directly from the fluorescent microscope. The graph's baseline intensity is not zero due to the background fluorescence picked up by the microscope. This is normal in fluorescent microscopy and can be eliminated while preserving the integrity of the data. Figure 16b) represents the data when background fluorescence is eliminated by subtracting the background intensity from each measurement. Background intensity was calculated individually for each data set by taking the average intensity in an area which contained no cells.

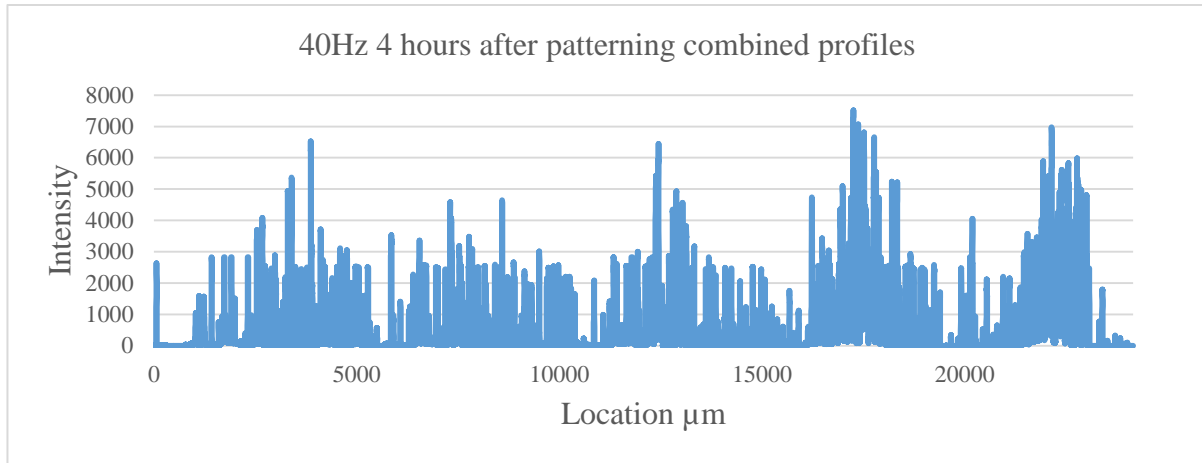


Figure 17 Combined fluorescent intensity data for 40Hz 4 hours after patterning

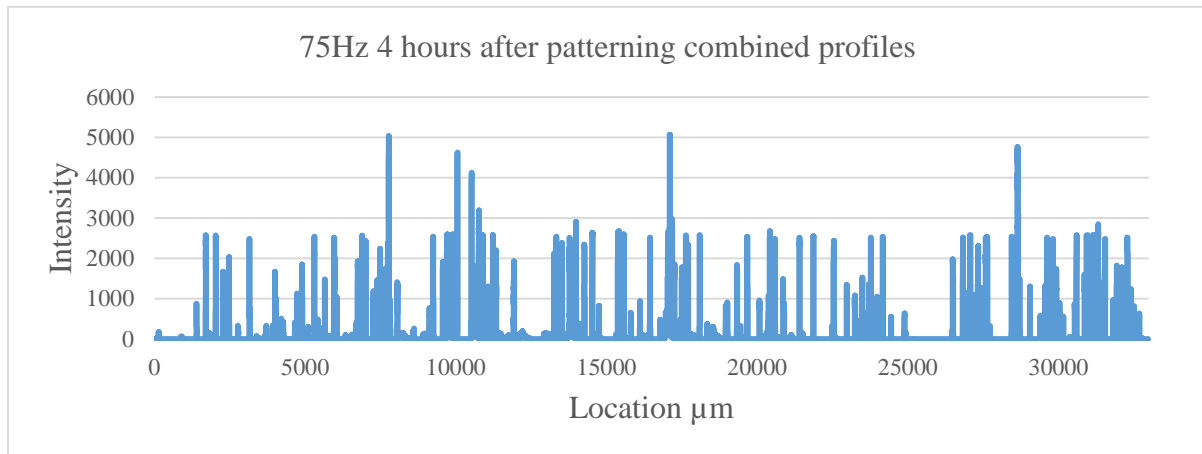


Figure 18 Combined fluorescent intensity data for 75Hz 4 hours after patterning

The original intent of this analysis was to take the average of each intensity value and plot it vs location. This would aid in gaining a better understanding of the location of patterned bands of cells, cell migration over time, and cell proliferation over time. Unfortunately this type of analysis did not prove fruitful. As seen Figure 17 Combined fluorescent intensity data for 40Hz 4 hours after patterning and Figure 18, when averaged the data becomes jumbled and does not represent the overall pattern created; likely due to a combination of the curvature of the pattern formed and intensity spikes between bands of cells due to individual cells outside of the patterned bands but within measurement fields. Thus, the idea of averaging intensity measured

was dismissed. Instead, the five 1 pixel wide fluorescent intensity measurements were compared intensity measurements over each day the samples were imaged.

In Figure 16, locations on the graph where the fluorescent intensity remains consistently high directly correlate to the patterned bands of clustered cells. Locations on the graph where the fluorescent intensity remains consistently low directly correlates to areas between the bands where cells were not patterned. As briefly stated before, there are spikes of high intensity measurements between the expected bands of cells, likely due to errant individual cells which were not successfully patterned.

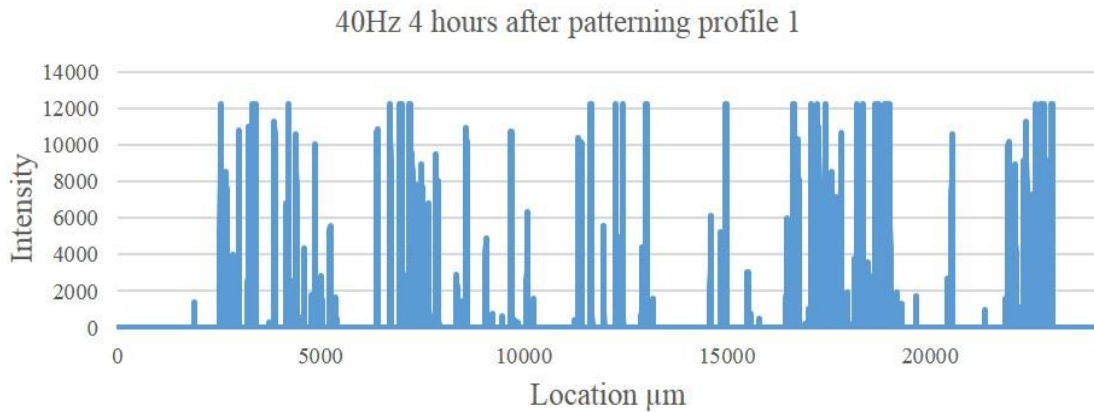


Figure 19 40Hz 4 hours after patterning. Location (1)

### 3.4.4 Cell pattern fluorescence data over length of the images

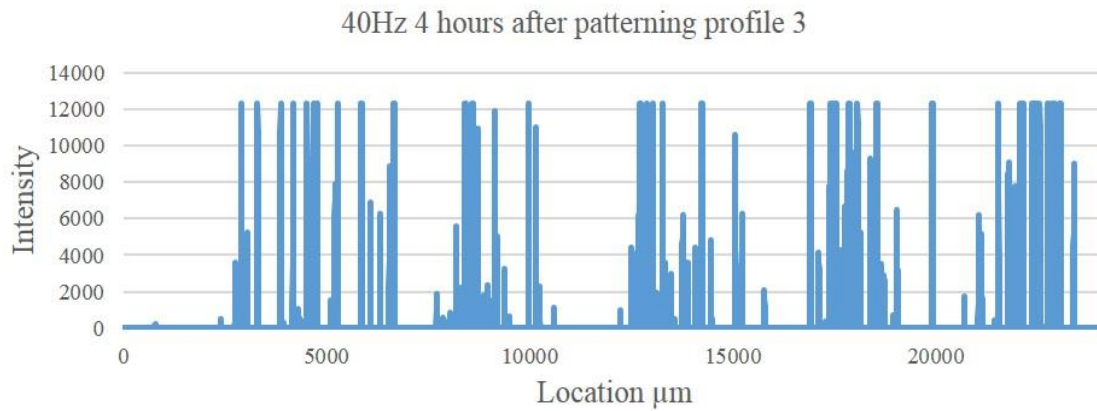


Figure 21 40Hz 4 hours after patterning. Location (3)

The following figures contain fluorescent intensity data over the length of the stitched images for cell patterns created using 40Hz and 75Hz. Data was normalized to remove background fluorescence, similar to Figure 16b.

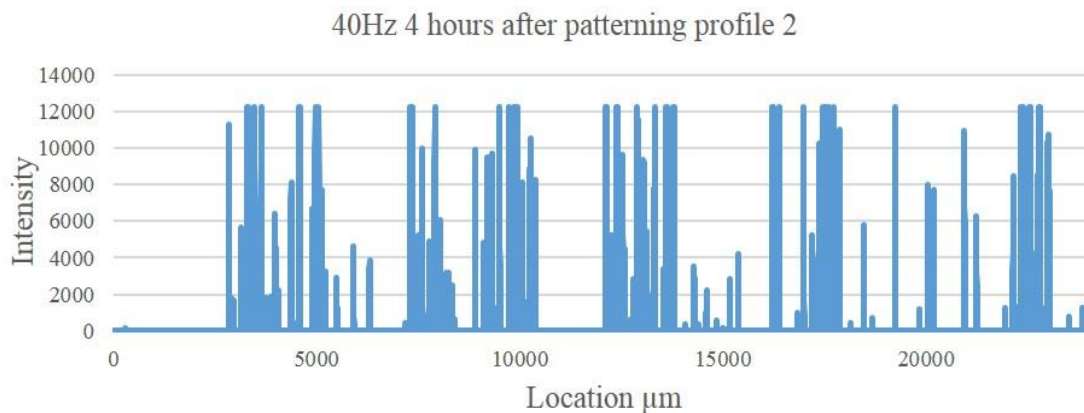


Figure 20 40Hz 4 hours after patterning. Location (2)

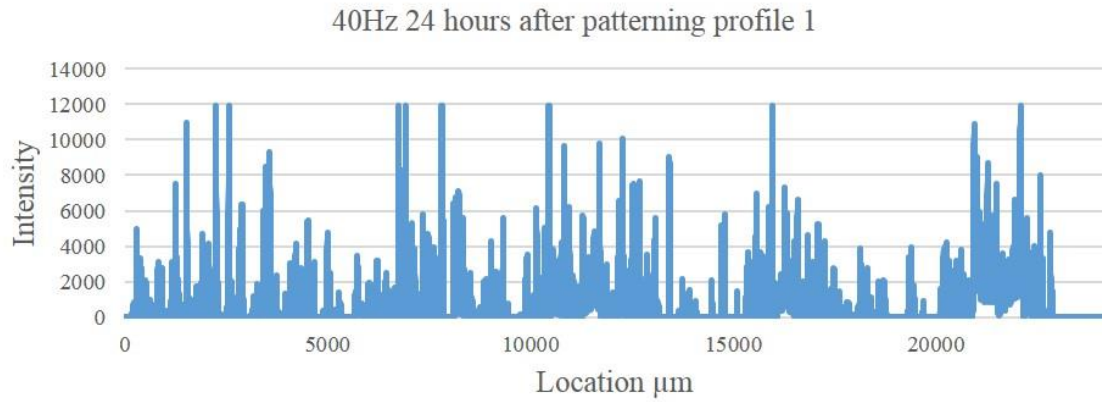


Figure 24 40Hz 24 hours after patterning. Location (1)

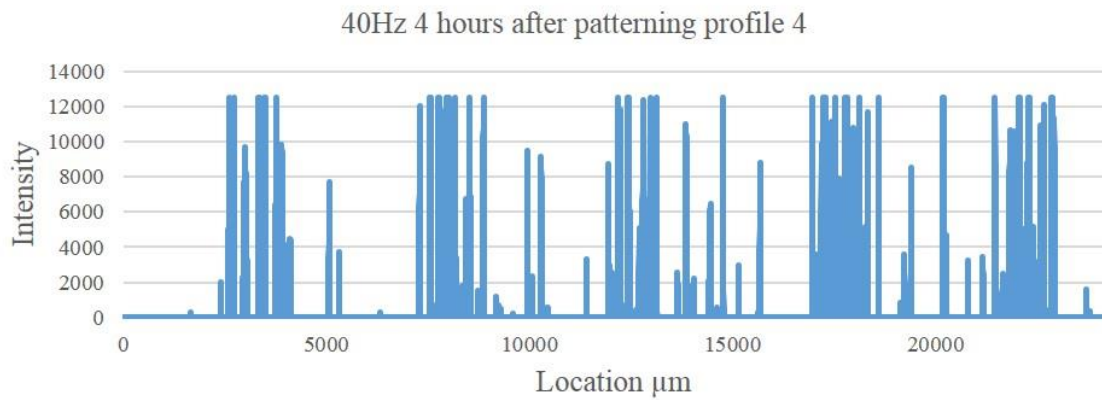


Figure 22 40Hz 4 hours after patterning. Location (4)

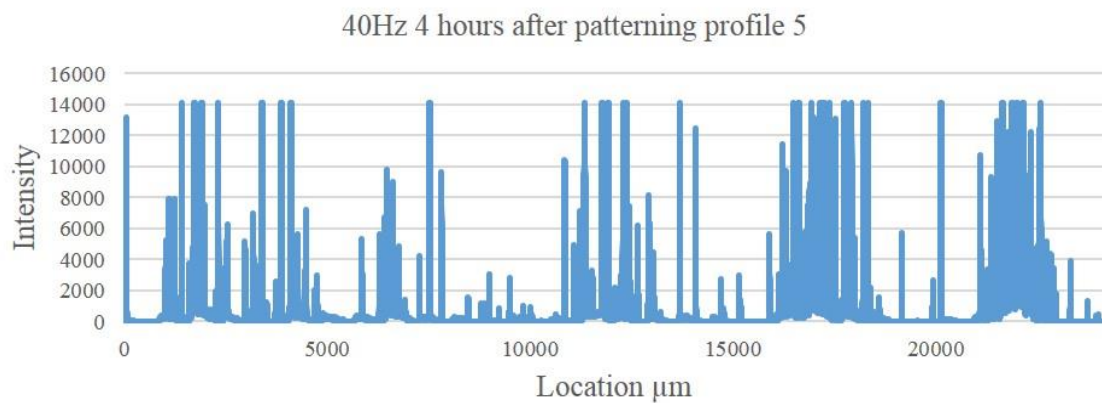


Figure 23 40Hz 4 hours after patterning. Location (5)



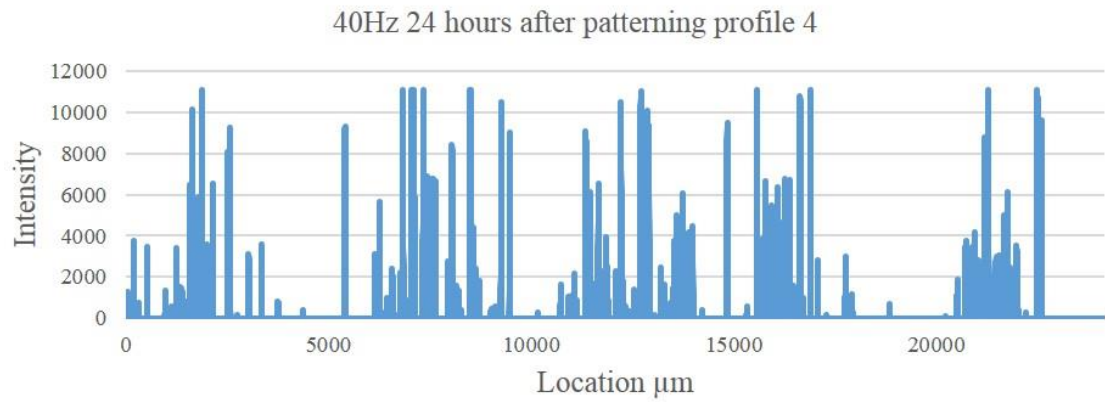


Figure 27 40Hz 24 hours after patterning. Location (4)

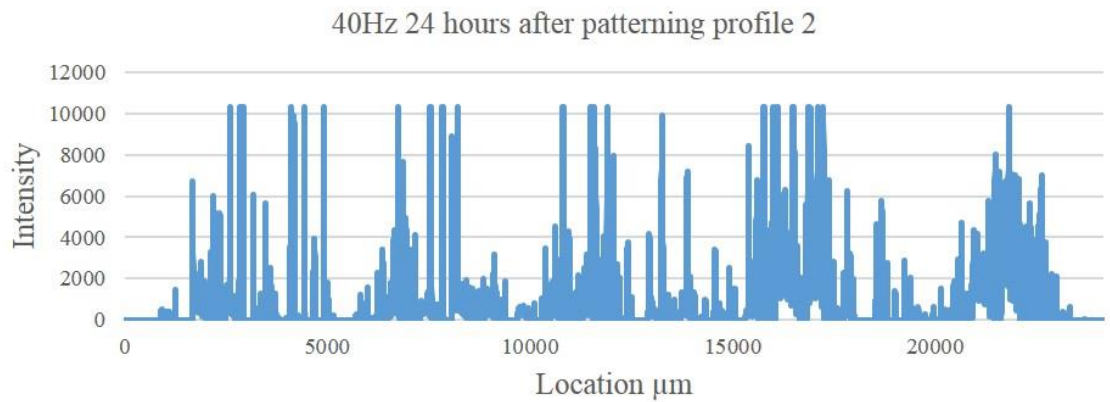


Figure 25 40Hz 24 hours after patterning. Location (2)

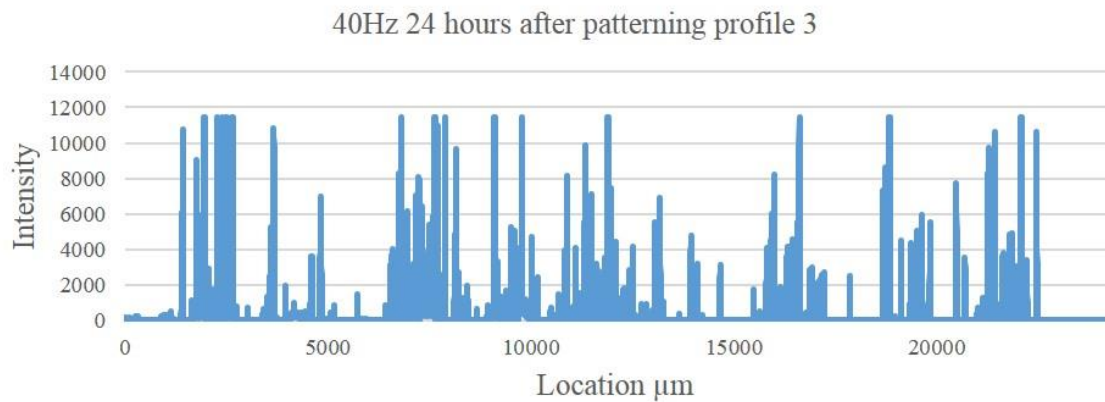


Figure 26 40Hz 24 hours after patterning. Location (3)

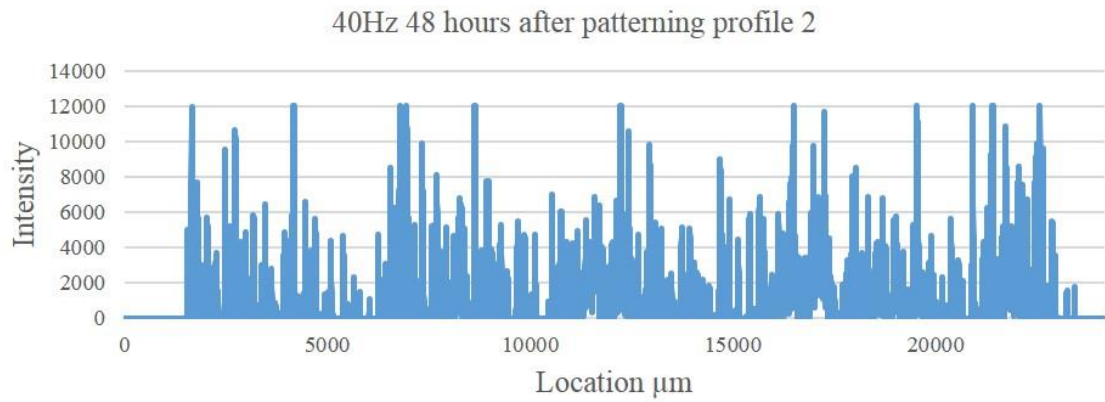


Figure 30 40Hz 48 hours after patterning. Location (2)

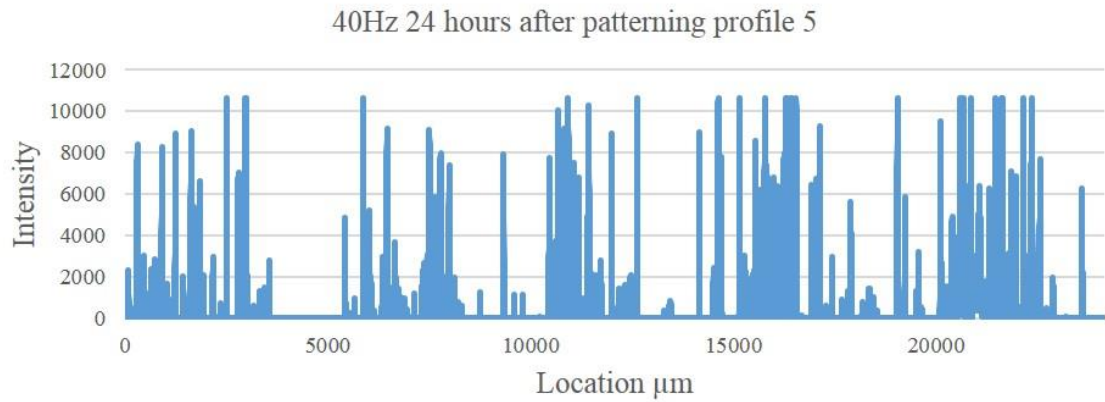


Figure 28 40Hz 24 hours after patterning. Location (5)

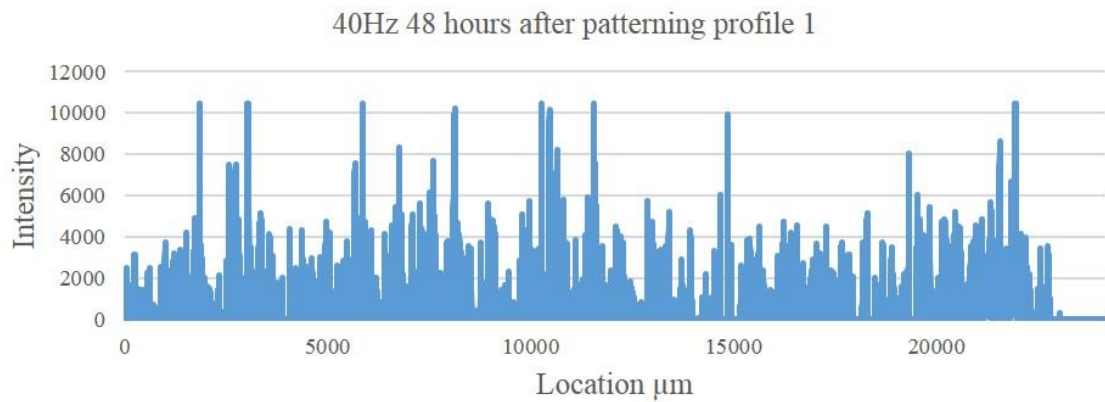


Figure 29 40Hz 48 hours after patterning. Location (1)

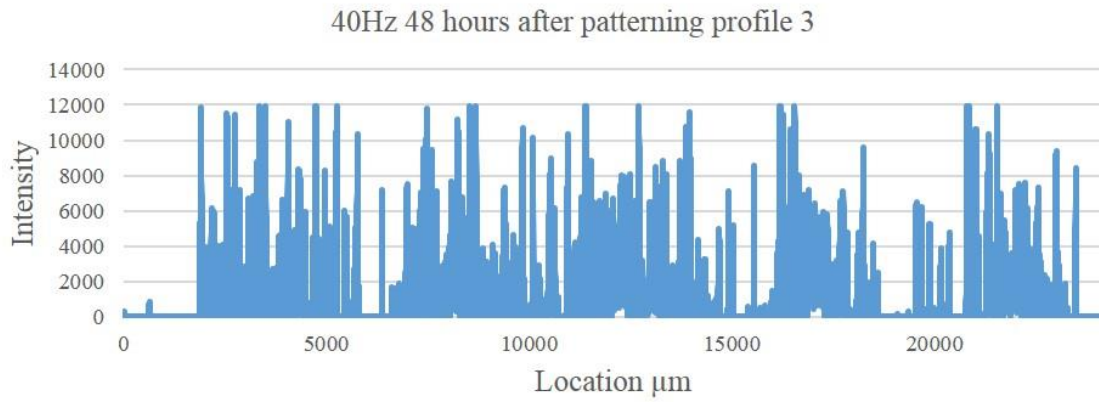


Figure 31 40Hz 48 hours after patterning. Location (3)

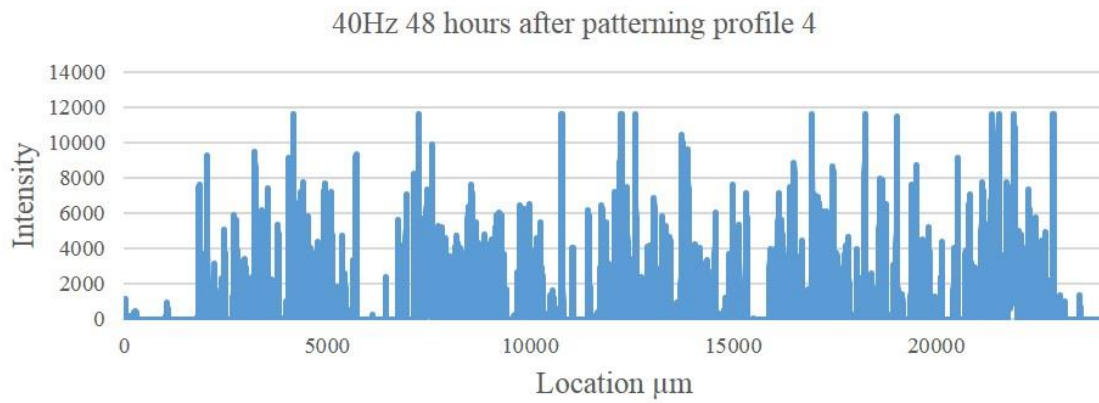


Figure 32 40Hz 48 hours after patterning. Location (4)

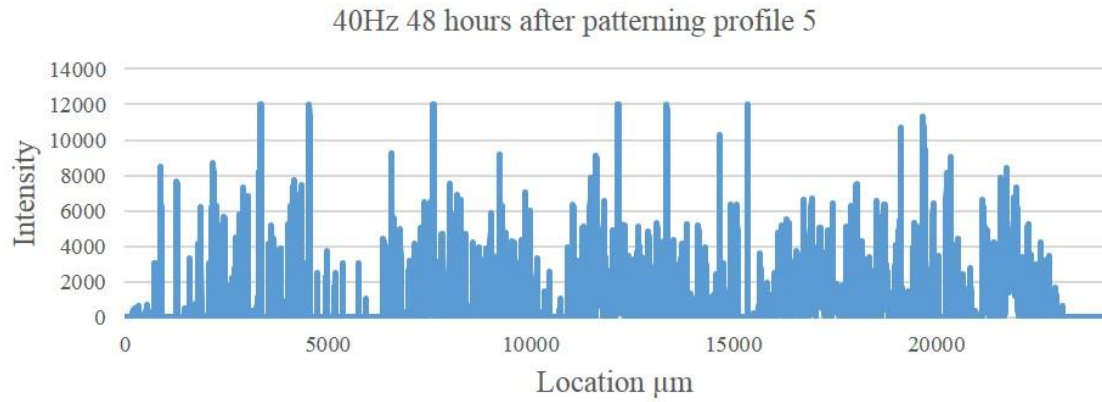


Figure 33 40Hz 48 hours after patterning. Location (5)

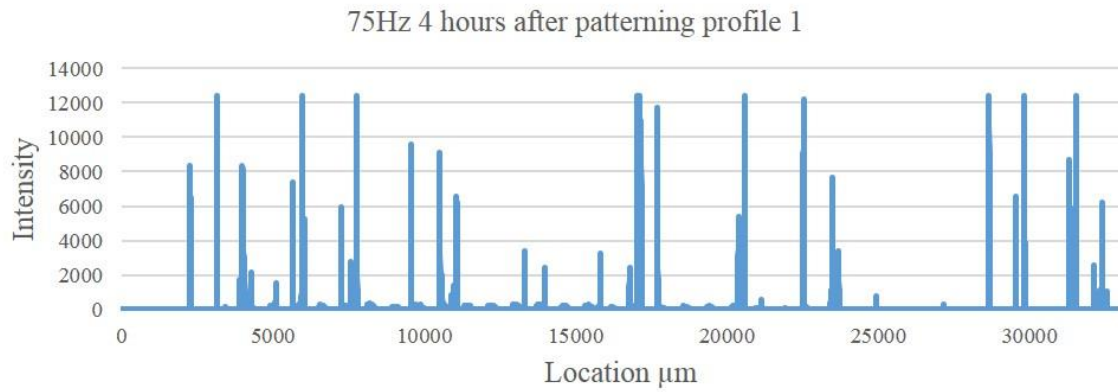


Figure 34 75Hz 4 hours after patterning. Location (1)

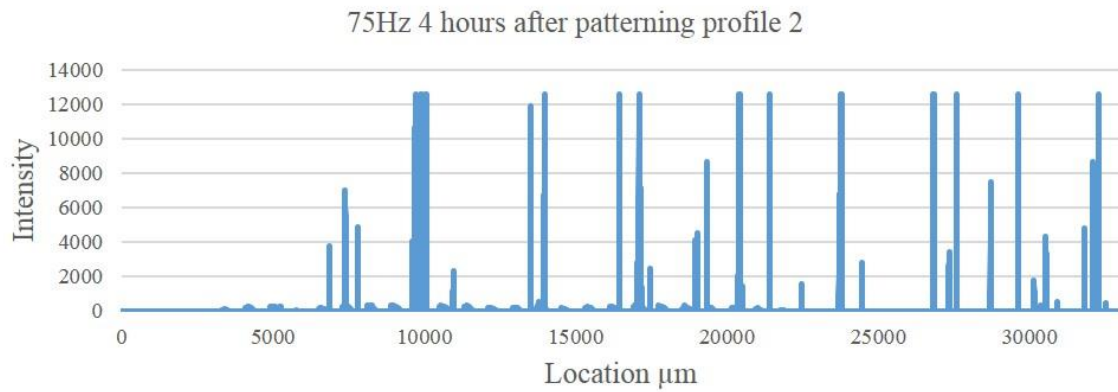


Figure 35 75Hz 4 hours after patterning. Location (2)

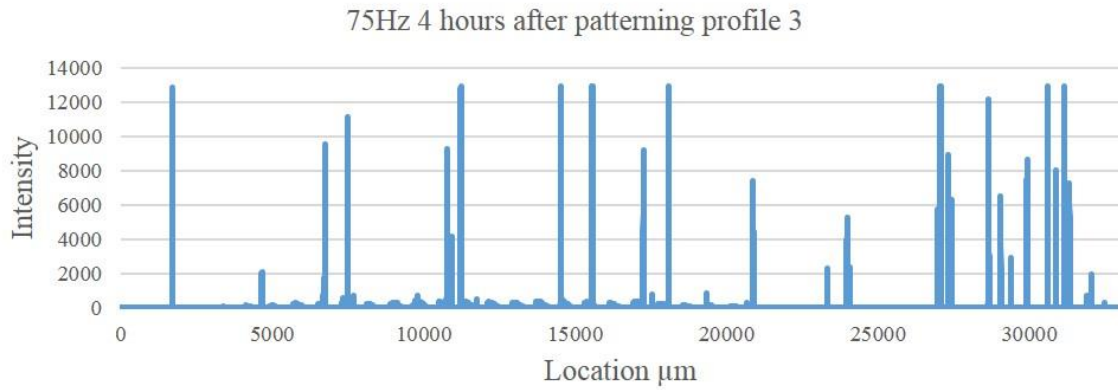


Figure 36 75Hz 4 hours after patterning. Location (3)

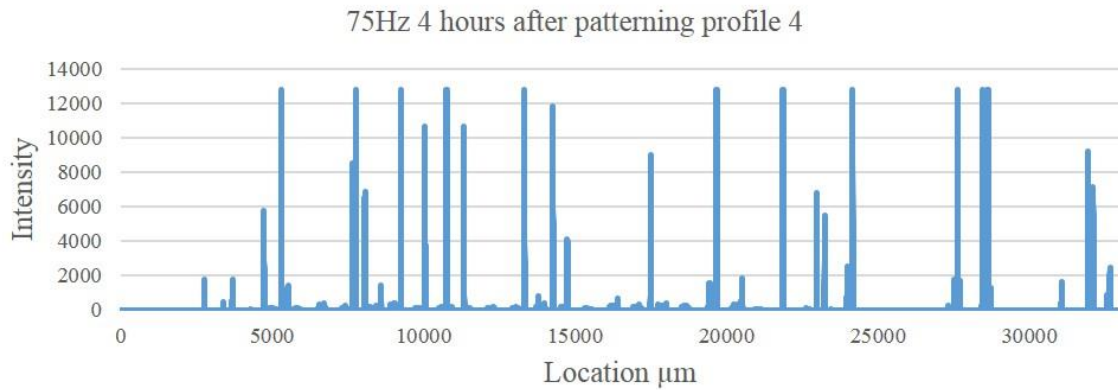


Figure 37 75Hz 4 hours after patterning. Location (4)

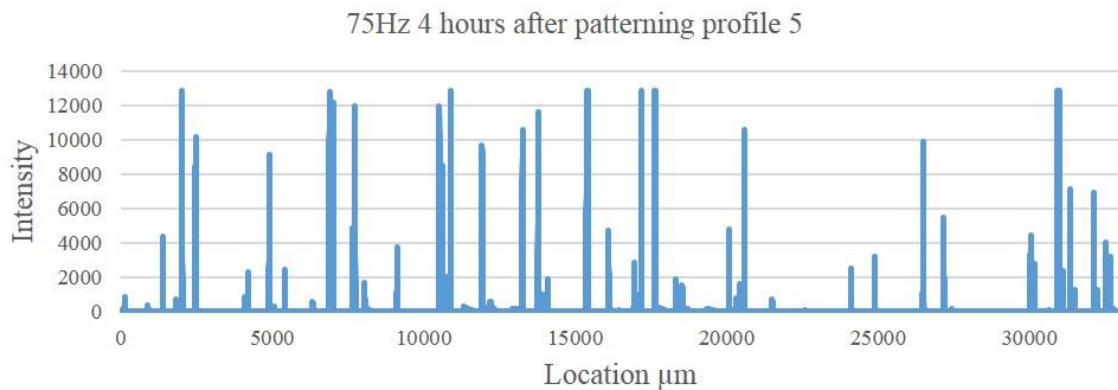


Figure 38 75Hz 4 hours after patterning. Location (5)

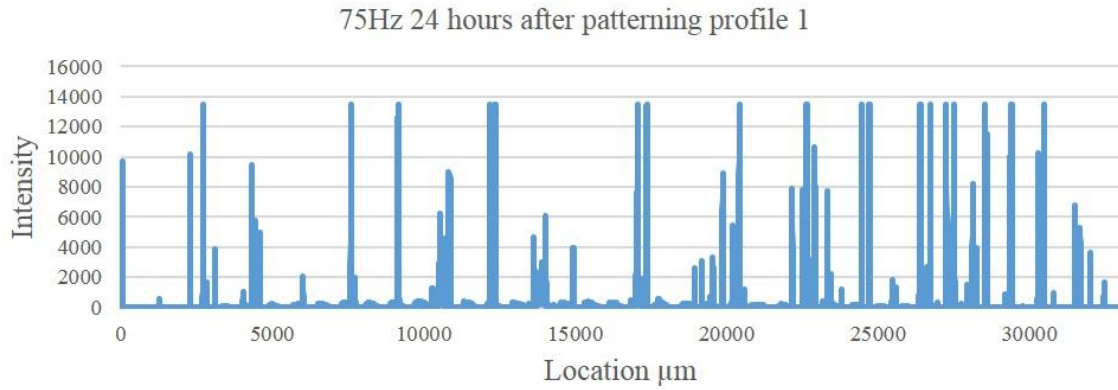


Figure 39 75Hz 24 hours after patterning. Location (1)

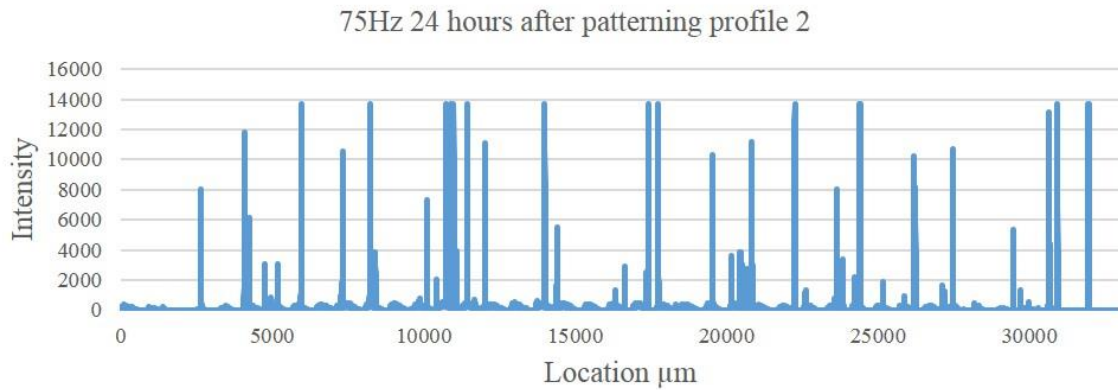


Figure 40 75Hz 24 hours after patterning. Location (2)

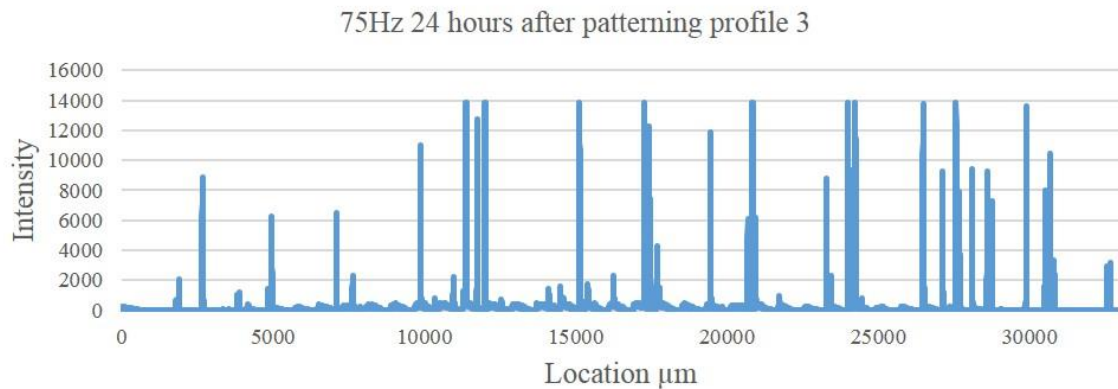


Figure 41 75Hz 24 hours after patterning. Location (3)

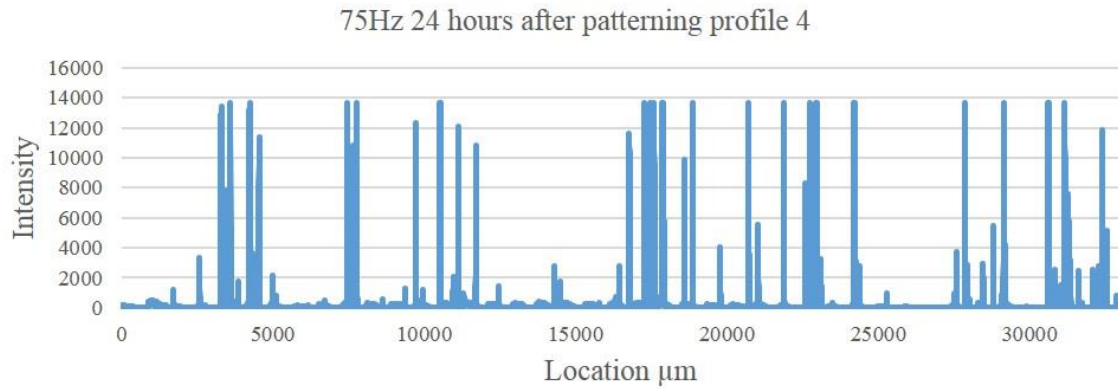


Figure 42 75Hz 24 hours after patterning. Location (4)

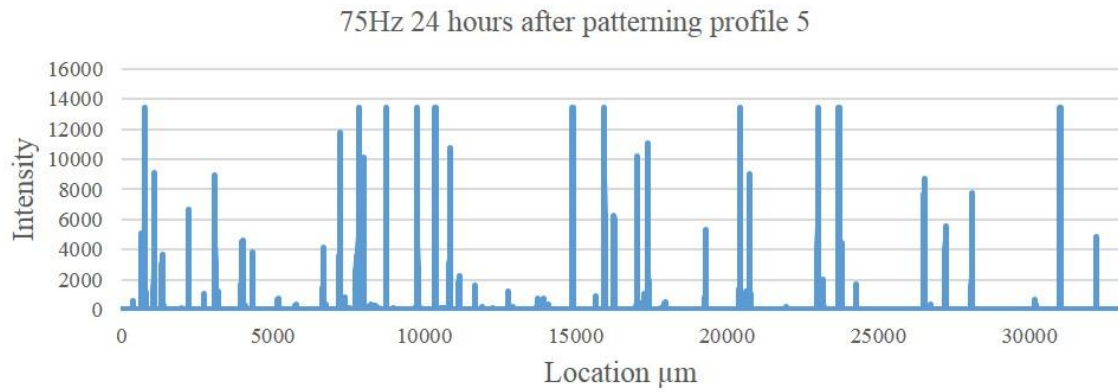


Figure 43 75Hz 24 hours after patterning. Location (5)

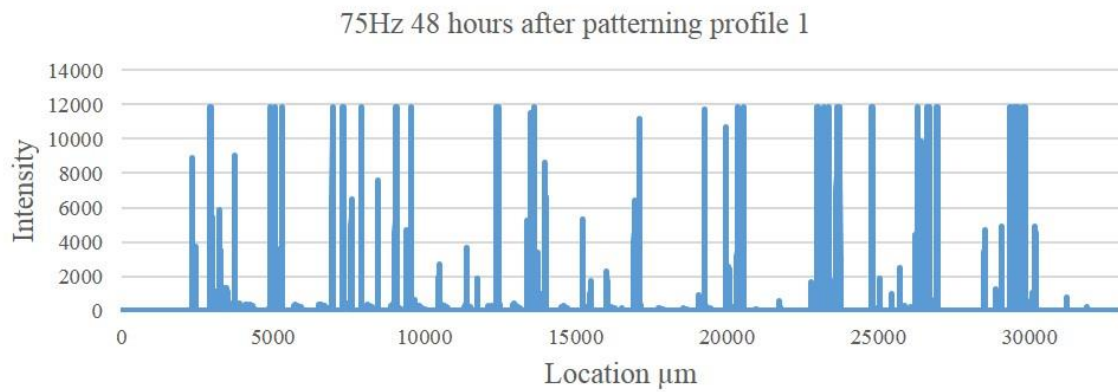


Figure 44 75Hz 48 hours after patterning. Location (1)

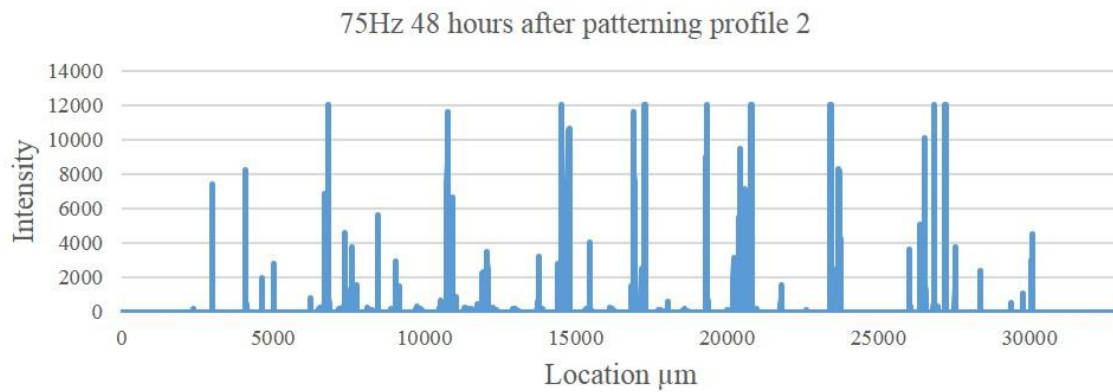


Figure 45 75Hz 48 hours after patterning. Location (2)

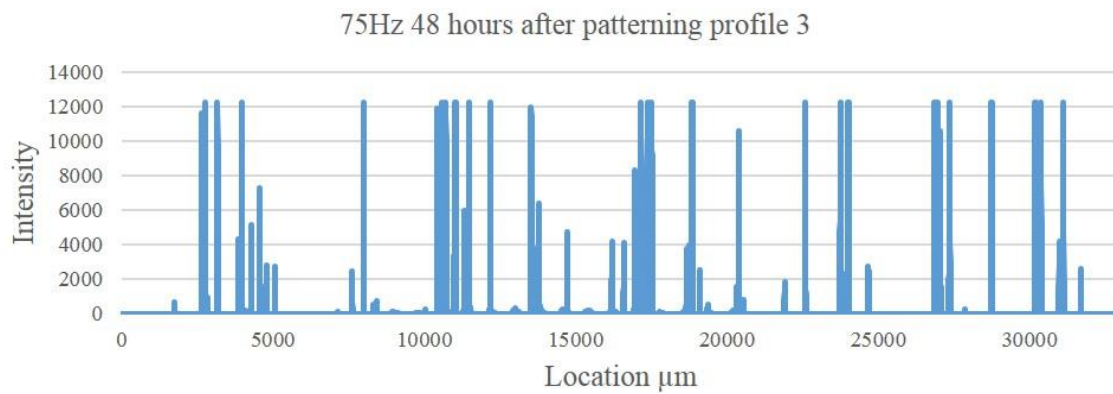


Figure 46 75Hz 48 hours after patterning. Location (3)

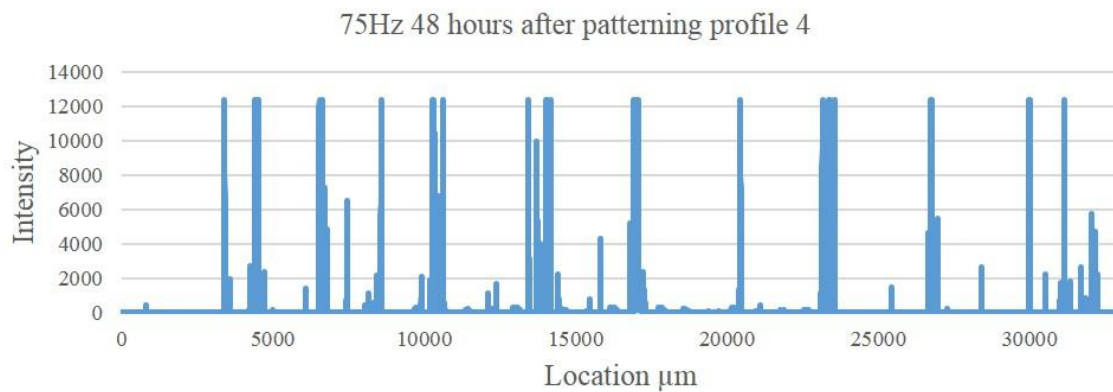


Figure 47 75Hz 48 hours after patterning. Location (4)



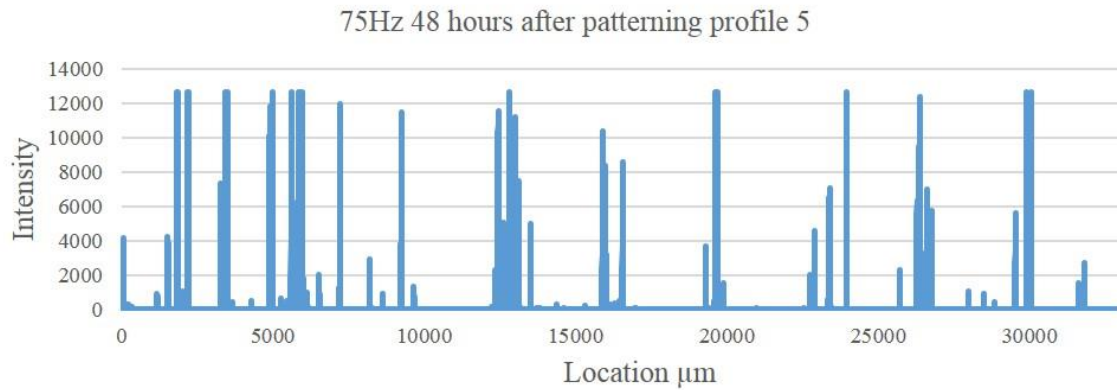


Figure 48 75Hz 48 hours after patterning. Location (5)

Figure 19 through Figure 33 represent the fluorescent image data gathered for 40Hz patterns using automated fluorescent microscopy. Figure 19 - Figure 23, 4 hours after patterning, all display 5 main peaks in fluorescent intensity. The location of each peak varies which is due to the curvature of the pattern formed. If the pattern created were truly symmetric and imaging was done perfectly then location pairs, such as location 1 and 5 or 2 and 4, should have intensity peaks at relatively similar locations. From these graphs, location 1 has peaks around 2000-5000 $\mu\text{m}$ , 6000-8000 $\mu\text{m}$ , 11000-13000  $\mu\text{m}$ , 16500-19000  $\mu\text{m}$ , and 22000-23000 $\mu\text{m}$ . Location 5 has peaks between 1000-4000  $\mu\text{m}$ , 6250-6750  $\mu\text{m}$ , 11000-13000  $\mu\text{m}$ , 16000-18500  $\mu\text{m}$ , and 21000-23000  $\mu\text{m}$ . The overall locations where intensity peaks is similar for location pair 1 and 5. Location pair 2 and 4 share peak locations around 3000-4000  $\mu\text{m}$ , 7500-9000  $\mu\text{m}$ , 12000-13000  $\mu\text{m}$ , 17000-18000  $\mu\text{m}$ , and 22000-23000  $\mu\text{m}$ . As expected, these results become harder to interpret as time passes. Over time the cells migrate and proliferate, leading to a blending of intensity peaks and making it more difficult to accurately determine where intensity peaks begin and end, as seen in 48 hours after patterning, Figure 29-Figure 33.

Interestingly, intensity profiles for 75Hz, all have distinct peaks with little noise. That being said, it still follows the trend of intensity peaks becoming wider as cells have time to

migrate and proliferate. This could be due to more accurate matching of the desired excitation amplitude at 75Hz than the excitation amplitude used at 40Hz. Neither input or output amplitude were directly measured for this study, future work should remedy this by measuring the force output at each frequency.

Initial band width differed in 40Hz and 75Hz, specifically 75Hz displayed a thinner initial band width than 40Hz. This can be visualized when comparing the representative Figure 12 and Figure 13 can be analyzed using the intensity profiles for each frequency. This coincides with one of the basics of vibrations: if frequency increases, wavelength must decrease.

### **3.5 Conclusion and Future Work**

In conclusion, this work demonstrates the feasibility of using vibrational forces to manipulate and pattern large numbers of cells at once. The patterns discussed, corresponding to the frequencies of 40Hz and 75Hz, here have no deleterious effects on NIH3T3 fibroblast viability, proliferation, or migration. Once cells are patterned in suspension and allowed to adhere to the surface of the tissue culture dish, the cells overall remain in that pattern for up to 48 hours. This work is the tip of the iceberg, it demonstrates two of the multitude of possible patterns and future work is highly encouraged. Further research into cellular patterning can be expanded by adjusting different factors such as:

- Frequency and/or amplitude of the vibrational force
- Changing the application point of the vibrational force to different locations on the dish
- Adding multiple contact points of the vibrational force
- Forcing nodal locations by damping specific points on the dish
- Size, shape, and/or density of the tissue culture dish

Overall, the experimental data gathered and presented within this section appears to fit a sinusoidal waveform; an expected result due to the sinusoidal vibrational force used during cellular patterning. While not within the scope of this study, a natural extension would be to analyze the data further and develop a mathematical model which matches the experimental results. This type of analysis could benefit an expansion of the computer modeling performed here.

Modeling and simulations performed for this study were used to predict the frequencies of mode shapes in air. While the model was not developed to predict modal frequencies with the addition of liquid, it could predict the types of mode shapes expected from experimental results. In order to further the development of cellular patterning and manipulation using vibrational forces, this model requires further refinement. Specifically, the model would greatly benefit from the addition of fluid-solid interactions, particle tracking, and a tunable sinusoidal force applied to the bottom of the tissue culture dish.

Further analysis of the cellular patterns developed in this work should be performed. Band width, the thickness of each band of cells that is produced, should be further characterized and specific boundaries of where a band begins and ends could be defined. This would assist in determining the relationship between band width and excitation frequency. Additionally, defining boundaries of the produced cell bands would aid in analyzing band-band encroachment due to cell migration and/or proliferation over time.

## Chapter 4: Key Findings and Future Work

The key findings of this dissertation are as follows

- Pressure waves generated by acoustic devices have an intermediate range which is acceptable for manipulating and patterning adherent cells.
- Power, energy, and intensity of acoustic pressure waves all have impacts on cell attachment and viability.
- An increase in power to an acoustic device will detach more cells from the surface in shorter exposure times at the cost of long term cell viability.
- Attached mammalian cells which are detached from a surface by sonication do not necessarily lyse or go through apoptosis.
- Simple vibrations can be utilized to pattern microscopic particles, including living mammalian cells in suspension.
- The addition of liquid to a vibrating dish causes pattern formation to become dependent on both frequency and amplitude of the vibration.
- Fibroblasts congregate at nodal locations when exposed to appropriate vibrational and acoustic forces.
- Once placed in a particular pattern while in suspension, adherent cells retain the patterned formation for up to 48 hours.
- Forces involved with the patterning described were low enough to not cause permanent damage to the cell as there was no significant cell death or loss of population.

- Cell population continued to grow, migrate, and proliferate once patterned.

## **4.1 Incomplete and Ongoing Work: Characterization of Cellular Mechanical Properties using AFM**

### 4.1.1 Background

Mechanical properties of cells are extremely important to many fields including tissue engineering, disease detection, and acoustic manipulation. Tissue engineers strive to develop new ways to repair or replace damaged tissues. To do this, the mechanical properties of individual cells and complete tissues must be known. Similarly, diseases, such as cancer, affect the mechanical properties of native cells [18, 56]. Studying these changes can lead to the development of early detection devices and new drug delivery mechanisms.

Currently there are multiple techniques to determine the physical characteristics of individual cells. Micropipette aspiration, first published by MITCHISON and SWANN [57], uses suction pressure to suck part of a cell into a micropipette. Mechanical properties are ascertained by observing the change in shape of the cell as a result of the suction pressure. Furthermore, this technique has been used to characterize membrane stiffness of both red blood cells [58] and leukocytes [59]. Optical traps, more commonly known as optical tweezers or laser tweezers, were developed in 1970 [60]. This technique uses a laser beam to exert small attractive or repulsive forces on dielectric particles. Since its development, optical tweezers have been used to trap viruses and bacteria [61], test optical deformability of red blood cells [62], and even observe protein folding in response to mechanical force [63]. Magnetic twisting cytometry evaluates cytoskeletal stiffness by measuring the rotation of cell membrane bound magnetic microbeads [64]. Atomic Force Microscopy (AFM), first developed by Binnig, et al. [65], has proven to be an extremely useful tool in the study of cellular mechanics. While AFM is a

relatively new technology, many scientists worldwide are utilizing its precise measurement capabilities to study processes never before possible.

Researchers have also used AFM to develop specific techniques in order to investigate specific cellular properties. One of these new techniques, dubbed single cell force spectroscopy (SCFS) [66, 67] utilizes AFM's precise measurement capabilities to investigate the adhesive force of cells between various surfaces and even other cells [66-68]. This is done by attaching a cell to the end of a tip-less AFM cantilever and using it as a living biological probe. However conventional SCFS does have its drawbacks. Because of the precise measurement capabilities, AFM is unable to generate large forces such as those required to remove cells after long term adhesion has taken place, restricting this technique to adhesion times within a few minutes.

#### *4.1.1.1 Cell Mechanical Properties: Elasticity and Natural Frequency*

Utilizing AFM, researchers have begun to investigate cellular elasticity [11-14]. However, these studies probed cells with sharp tipped cantilevers and reported varying stiffness values at different locations of the cell [14]. Data reported by Mathur, et al. [14] demonstrates that measurements made over the nucleus are significantly stiffer than those made over the cell body. The inconsistencies of reported stiffness values along with indentation ranges of only a few hundreds of nanometers give poor insight into the overall stiffness of the cell.

Natural frequency of an object can be defined as the frequency, or sets of frequencies, an object vibrates at when disturbed. This basic physical principal applies to all structures including biological organisms. Excitation of an object at one of its natural frequencies causes that object to accumulate energy; if the energy is not dissipated the object's structure can become unstable and permanent damage can ensue. While this could be advantageous for targeted disease treatments, it could also be disastrous for tissue construction. Multiple studies have used models

to predict cell natural frequencies [69-73] but there is insufficient research into the experimental verification of the natural frequencies of cells.

This research proposes a rethinking of cellular stiffness into both global, over the entire cell, and local, at a specified location, stiffness. Under this definition previous research using tipped AFM cantilevers would fall under local stiffness measurements. The work proposed here would fall under global stiffness which could depend on multiple factors including cytoskeletal composition and cell shape. Certainly if global cell stiffness is an amalgamation of its internal components and overall shape, it stands within reason that a cell's natural frequency would also depend on these factors.

#### *4.1.1.2 Cytoskeletal Composition and Cell Shape*

The cytoskeleton is vital to eukaryotic cells and assists in multiple cellular activities including cell division, intracellular nutrient transport, and even helps regulate cell shape and mechanical properties[42]. It does this through the dynamic disassembly and reassembly of three main protein structures known as microfilaments, intermediate filaments and microtubules. Microfilaments, also known as actin filaments, generate contractile forces within a cell through a myosin motor moving along actomyosin fibers. Actin filaments can also create protrusions against the cell membrane; these protrusions have been reported as being stiffer than surrounding locations most likely due to the high concentration of actomyosin bundles in the area [13]. Intermediate filaments are mainly used within the cell to anchor organelles within the cell's structure and to structurally support the nucleus. Finally, microtubules, the largest of the three cytoskeletal structures, assist the cell in counterbalancing actin filaments by resisting compression.

As previously discussed, studies of cellular stiffness utilizing AFM have made small indentions into the cell [11-14]. These local measurements likely correspond to the cell membrane and the cytoskeletal configuration immediately below. These reports, combined with the current gap in literature on cellular global stiffness, fail to investigate how the major cytoskeletal elements contribute to the cell's overall properties.

Along with cytoskeletal composition, cell shape plays a major role in regulating the cell's mechanical properties [11, 42]. Mammalian cells naturally take different shapes depending on their function. For example epithelial cells will restrict their shape by tightly packing together to form a protective barrier while fibroblast cells generally spread out and relocate to produce extracellular matrix components where needed. Analogous to cytoskeletal composition, current literature does not delve into how a cell's shape contributes to its global properties.

#### *4.1.1.3 Objectives*

The goal of this research was to cover three main objectives. The first objective was to experimentally measure individual cell stiffness using both a technique developed in Dr. Hasegawa's Micro-Nano Control and Biorobotics Laboratory [74, 75] and a new technique similar to SCFS using AFM. Stiffness values obtained through the nano-indentation technique would have been used to verify the validity of measurements made using AFM. Once verified, the AFM will also be used to investigate a cell's natural frequency, a mechanical property which has previously not been experimentally investigated.

The second objective was to use the developed measurement technique to further characterize a cell's stiffness and natural frequency. Currently it is unknown how a cell's shape or internal structural composition affect its global stiffness. To test these factors, individual cells would either be exposed to one of four biochemical factors which influence specific properties of



the cytoskeleton: serum-free media, Y-27632, nocodazole, or sodium azide, or be confined to a specified adhesion area developed through microcontact printing [42, 76, 77].

The final objective of this research was to characterize a second cell type's stiffness and natural frequencies using the developed AFM technique. It is important to ensure the developed technique is applicable to multiple cell types as the mechanical properties of cells differ corresponding to the role and shape of the cell. Additionally, this second cell type's stiffness and natural frequency were going to be examined after either exposure to the biochemical factors listed above or confined via controlled protein binding sites.

#### 4.1.2 Methods and Materials

##### 4.1.2.1 Cell Culture and Reagents

NIH3T3 murine embryonic fibroblasts (CRL-1658, ATCC) cultured in complete growth medium (CGM) containing 10% new born calf serum and 1% penicillin-streptomycin in Dulbecco's modified Eagle's medium. Cells will be passaged every three days using 0.25% trypsin-EDTA and used between passages 5 and 20.

Cell fixation was performed by adding 500uL of 4% paraformaldehyde in PBS to the growth media for 2 minutes, preventing cell damage from abrupt change in osmolarity. The media was then aspirated and rinsed with PBS before covering the cells in a 4% paraformaldehyde in PBS solution and incubated for 15 minutes at room temperature. A final aspiration and rinse in PBS was performed before experimentation.

#### 4.1.2.2 Fabrication of Microcontact Printing Stamp

First a glass slide was cleaned and sterilized by sonicating in acetone, methanol, isopropanol, and DI H<sub>2</sub>O for 10 minutes each followed by rinsing in flowing DI H<sub>2</sub>O for 30 seconds and blown dry using compressed N<sub>2</sub>. The slide was then baked on a hot plate at 250°C for 30 minutes to remove any excess water from the surface. Following this, the slide was placed under a glass container on a hot plate at 150°C. 3ml of HMDS was evaporated under the glass container for 15 minutes; forming a thin hydrophobic layer on the slide which improves photoresist adhesion. AZ 5214E was spun onto the slide at 2000 rpm to achieve a thickness of 2µm and soft baked at 105°C for 50 seconds before exposure. A table-top micro pattern generator (Heidelberg instruments µPG 101) was used to expose the desired pattern directly. This micro pattern generator acts similar to a printer. The UV light is mounted on a movable head which exposes the photoresist based on a specified pattern; this is advantageous because multiple patterns can be fabricated without the requirement of a mask. The photoresist was then submerged in NMD 3 developer for 50 seconds under gentle agitation to etch away the exposed resist. Etching was neutralized by submerging in DI H<sub>2</sub>O for 30 seconds and blown dry. Pattern

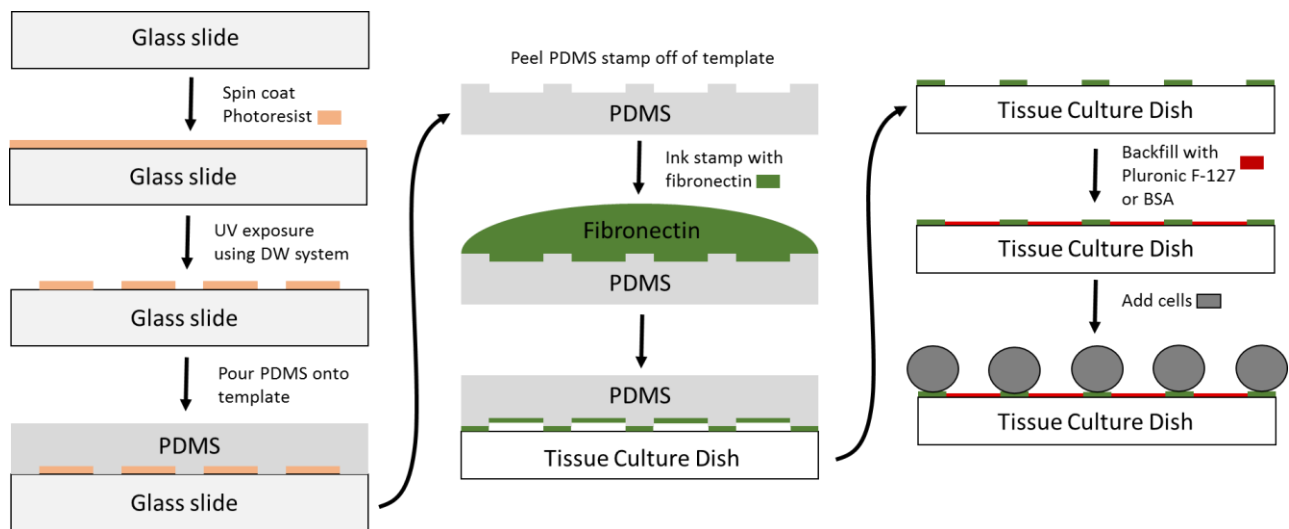


Figure 49 Fabrication of microcontact printing stamp and stamping procedure.

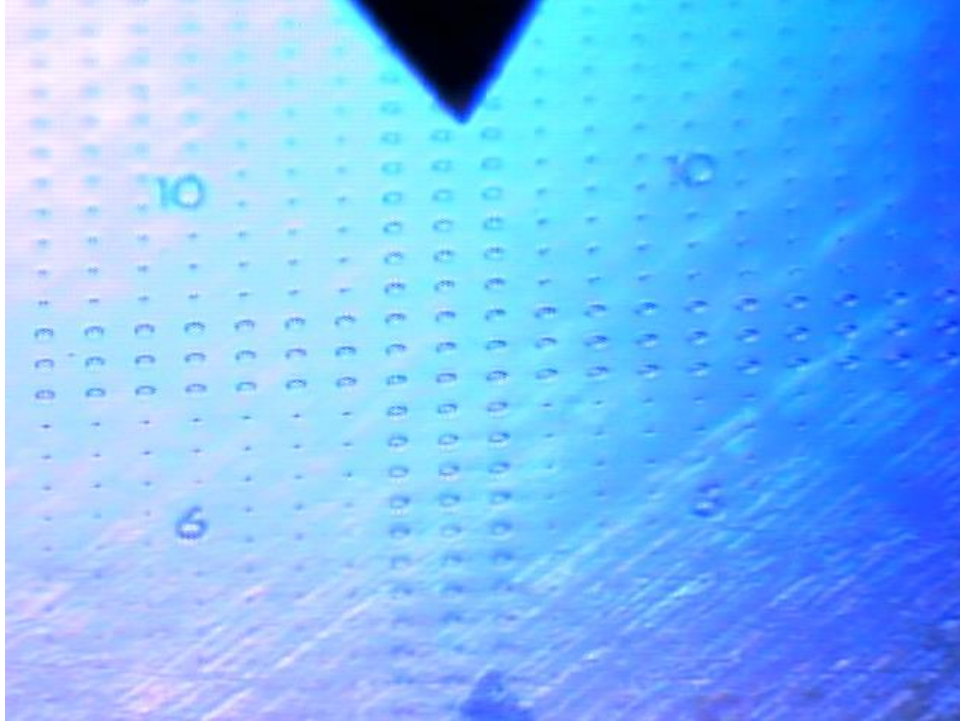


Figure 50 Surfcoorder ET200 used to verify etch depth of photoresist

fidelity was assessed via optical microscopy and surface measurements were taken using a Surfcoorder ET200. PDMS was mixed at a 10:1 ratio, poured over the photoresist template to achieve a thickness of 5mm, degassed under vacuum, and cured at 65°C for 2 hours. Once curing was complete and the PDMS cooled down to room temperature it was carefully peeled off of the photoresist template and trimmed appropriately.

#### *4.1.2.3 Microcontact Printing Procedure*

The microcontact printing procedure took place within a biosafety cabinet and all materials were sterilized prior to starting. The PDMS stamp was sterilized via sonication in ethanol for 10 minutes, followed by second sonication in DI H<sub>2</sub>O for 10 minutes, rinsed in flowing DI H<sub>2</sub>O for 30 seconds, blown dry with N<sub>2</sub>, and finally exposed to UV light for 15 minutes. Once sterilization was complete, one drop of 50µg/ml FN in PBS was placed onto the stamp and gently spread over the surface. The protein coated stamp was covered for 30 minutes, allowing the FN to adsorb from the solution onto the surface of the PDMS stamp. After, the

remaining FN solution was aspirated off, the stamp was immediately triple rinsed with PBS, and immediately dried using compressed N<sub>2</sub>. Using tweezers, the stamp was inverted and the protein covered microstructured surface was placed in contact with the desired substrate. Gentle pressure was applied with the tweezers to the back of the stamp to ensure conformal contact between the stamp and the surface. The stamp was left in contact with the surface for 1 minute to ensure FN transfer before carefully removing, making sure not to cause roof collapse upon removal. Once the stamp was removed it was submerged in H<sub>2</sub>O to keep the microstructures intact. The patterned substrate, in this case a clean and sterilized glass slide, was backfilled with either 0.2% (w/v) Pluronic F-127 in PBS for 1 hour or 1% heat denatured BSA in PBS for 1 hour. Backfilling is done to block non-specific binding sites on the surface of the glass, ensuring pattern fidelity. The surface was then rinsed with PBS, cells seeded onto the surface at 10,000 cells/cm<sup>2</sup>, and incubated for 2 hours. After 2 hours the excess unattached cells were removed using a gentle flow of fresh media from one side of the dish and aspirated off from the opposite side.

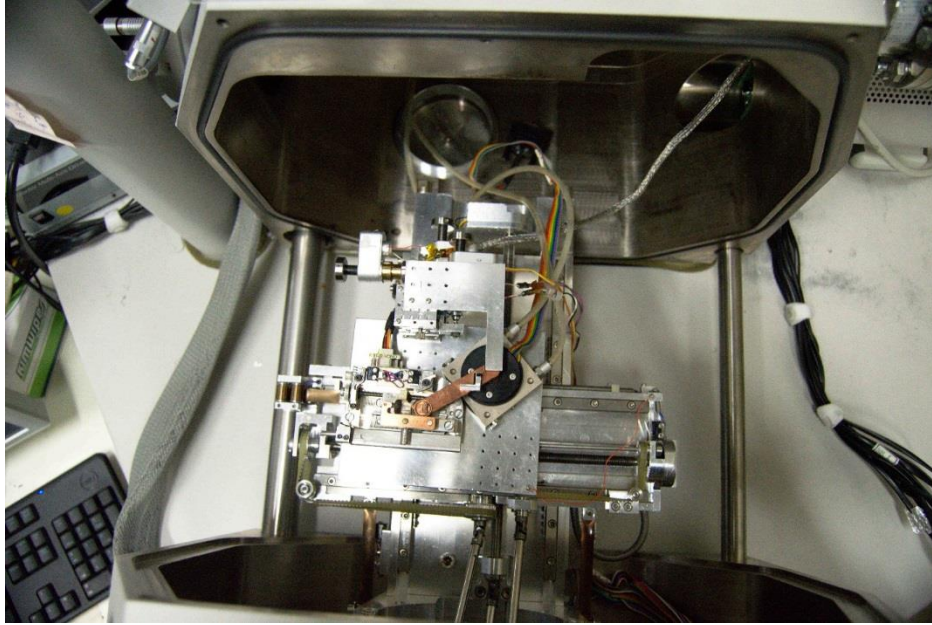


Figure 51 Nano-robotic manipulation system inside ESEM

#### 4.1.2.4 Experimental Procedure

Initial characterization of the tip-less AFM cantilevers was performed using the nano-robotic manipulation system, shown in Figure 51, developed in the Micro-Nano Control and Bio-Robotics Lab [74, 75]. This process was performed in real time using an environmental scanning electron microscope (ESEM) and a reference cantilever of known stiffness. The two cantilevers

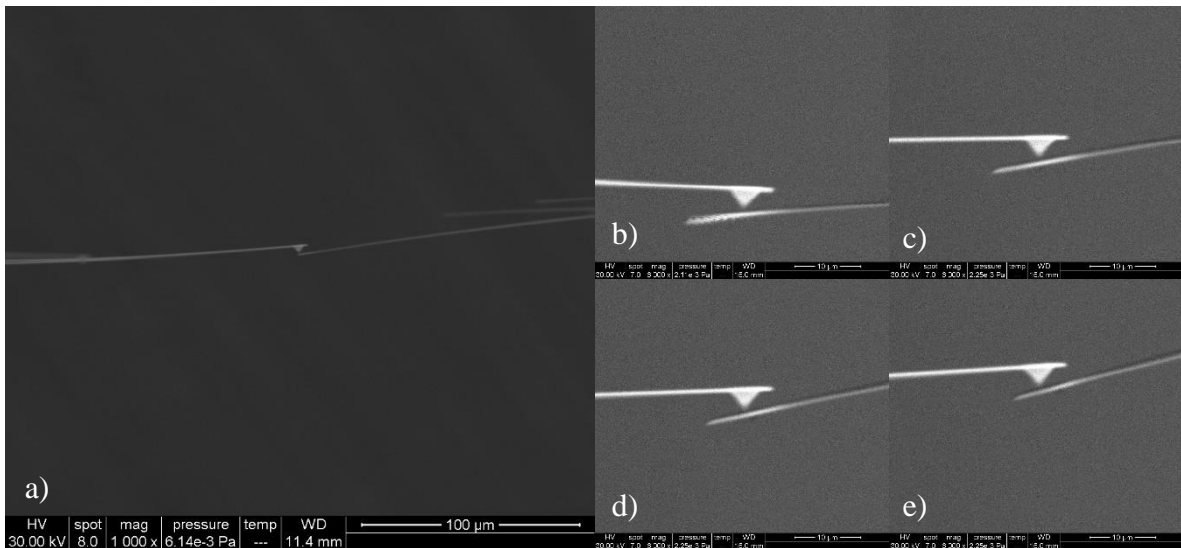


Figure 52 ESEM images of AFM cantilever calibration. a) reference cantilever in bending with tipless cantilever. b) reference cantilever making contact c) beginning of bending d) continuing bending e) final point for measurement

were brought into initial contact Figure 52b and carefully pressed against each other until elastic deformation occurs Figure 52e. In this configuration the cantilevers are in equilibrium and can be used to calculate the unknown cantilever's stiffness.

Characterization of the tip-less AFM cantilevers was also performed using AFM. While ESEM setup can only be used to measure stiffness, AFM can easily derive both cantilever stiffness and natural frequency. Cantilever natural frequency was found from a fast, simple, and convenient technique commonly used in AFM called a frequency sweep. A frequency sweep is when the AFM cantilever is excited through a range of frequencies; cantilever natural frequency was easily identified as the frequency with the greatest amplitude. Previous work has shown that the stiffness of the cantilever can be calculated from thermal data generated by thermal tuning [78, 79]. This method of calculating beam stiffness has multiple advantages over other methods as demonstrated by Burnham, et al. [78]. Recent work has increased the accuracy of these beam stiffness measurements to within 3-4% for beams with spring constants up to 50 N/m [80].

After cantilever characterization, limited cell measurement experiments were performed on the AFM. Cells initially were patterned using the microcontact printing stamps to control cell contact area and fixed for ease of use. Previously in Dr. Hasegawa's lab this nano-robotic manipulation system inside ESEM has been used to study yeast cell stiffness [81]. A similar procedure was attempted to measure fibroblasts cell stiffness. Mammalian cells cannot survive for very long in the harsh environments created inside the ESEM. To circumvent this issue, cell elasticity measurements were performed on dead cells which were fixed in a 4% paraformaldehyde PBS solution. The fixation process likely increases cellular stiffness due to the paraformaldehyde crosslinking proteins together and were noted when beginning AFM stiffness measurements\

## 4.2 Limited Results

Results from this research are limited which is why this is ongoing and future work.

### 4.2.1 Microcontact Printing Direct Proteins

Fabrication of stamps for microcontact printing was integral in controlling cell adhesion sites. Multiple different molds were successfully fabricated, one of which is shown in Figure 50. Although roof collapse was an ongoing issue, eventually a successful mold and stamp was created. Figure 53 shows successful direct fibronectin transfer from the PDMS stamp to a clean glass slide. After the protein was printed onto a surface it was blocked with Pluronic F127 to

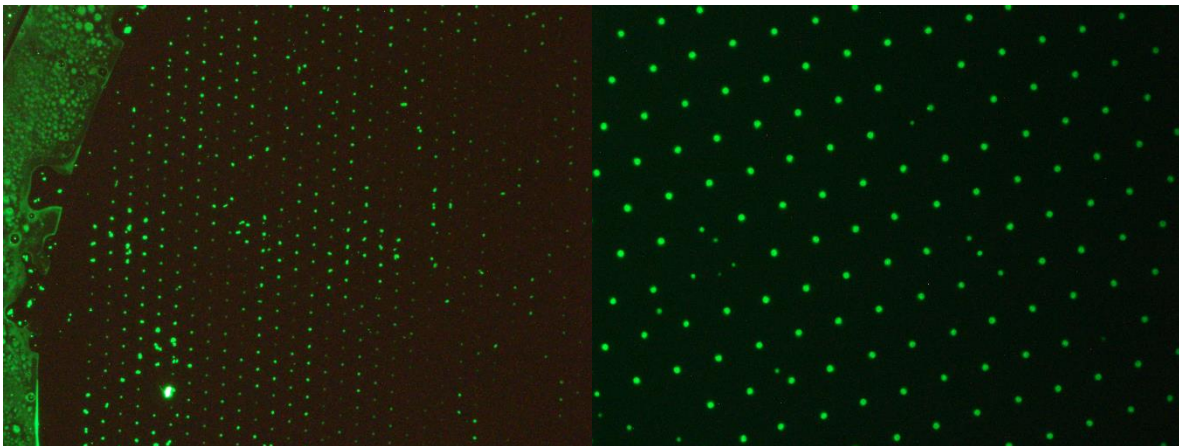


Figure 53 Green fluorescent fibronectin stamped onto a clean glass slide. a) 6 $\mu$ m b) 10 $\mu$ m

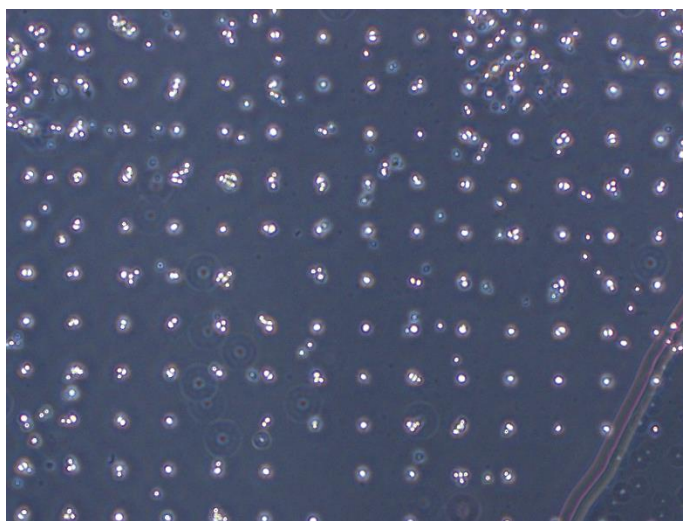


Figure 54 Successful cell attachment to fibronectin islands

prevent non-specific protein adhesion. Figure 54 displays an example of cells adhering to the fibronectin islands.

#### 4.2.2 ESEM Analysis of Mammalian Cells

Normally spread NIH3T3 Fibroblasts were fixed and prepared for imaging using ESEM. After fixation cells were triple rinsed with DIH<sub>2</sub>O to ensure no salt crystals would form in the vacuum environment of the ESEM. Figure 55 shows the results of ESEM imaging on a fixed fibroblast as the pressure decreases. In part a) the cell is barely visible at a pressure of 700 Pa. Decreasing the pressure greatly increases image quality of the fibroblast until Figure 55e) when the pressure reaches 210 Pa and the cell becomes damaged. Based on these limited results it is possible to image mammalian cells using ESEM if the pressure is kept above 350 Pa with good results achievable at 500 Pa.

Using these results, the next step was to attempt and deform a fibroblast using a tipless AFM cantilever. Figure 56 shows one attempt at bringing a cantilever in contact with a cell. Due

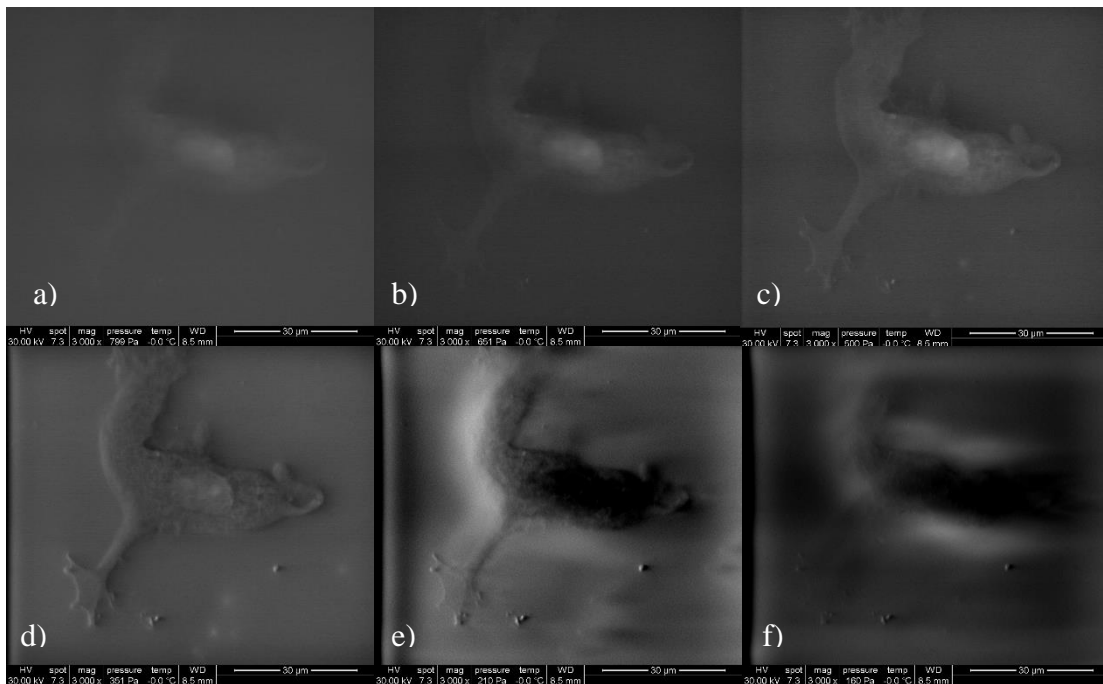


Figure 55 NIH3T3 fibroblast imaged using ESEM. a) 799 Pa b) 651 Pa c) 500Pa d) 351 Pa e) 210 Pa f) 160 Pa



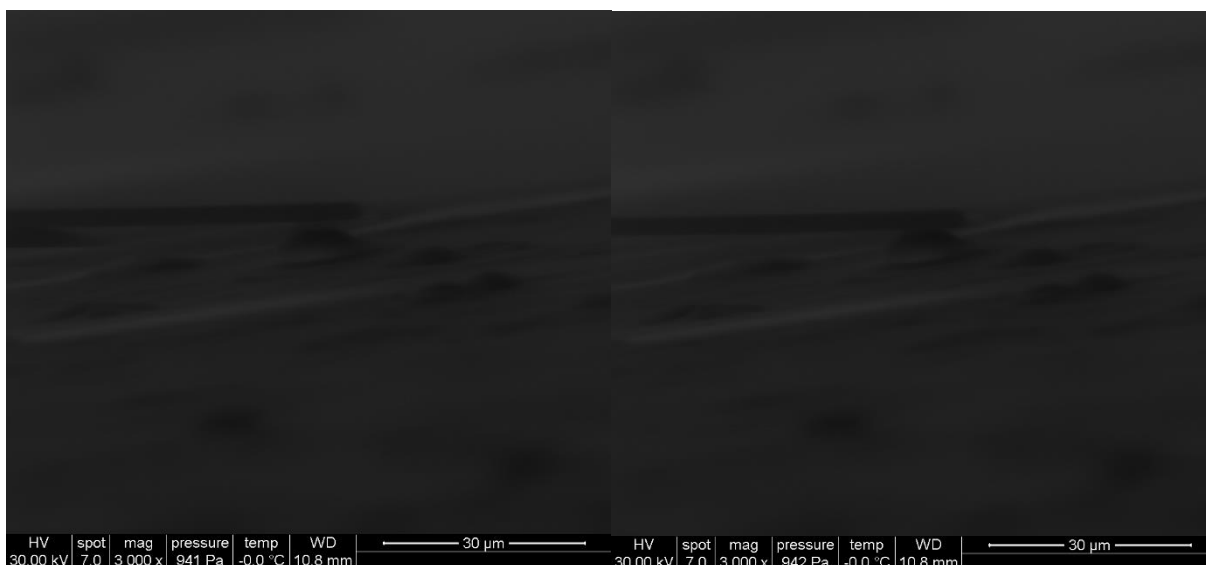


Figure 56 ESEM cell elasticity using tipless AFM cantilevers. a) approaching contact b) in contact

to either the fixation process, dehydration from the ESEM atmosphere, or a combination of the two, the cells would either refuse to deform or pop like a bubble immediately. Unfortunately there were not enough trials to gather reliable data from this research.

### 4.3 Conclusion and Future Work

In conclusion, even though this research was not finished it was still a valuable learning experience. This project granted hands on experience with AFM, ESEM, and microcontact printing, important tools in modern research.

#### 4.3.1 Future Work: AFM and Cytoskeletal Inhibitors

Future work will continue investigating the objectives and experiments outlined above. Specific interests lie in atomic force microscopy measurements of cells under four different factors, serum free media, Y-27632, nocodazole, and sodium azide. These four different factors have been shown to affect the adhesion force of cells; hypothesizing that if adhesion force is modified, elasticity of the cell should change as well. The first factor, serum-free media, chosen because serum contains growth factors required by the cell to assemble internal mechanisms which control adhesion [38, 77]. Studying cells in serum free conditions will show if these

growth factors affect cell stiffness as well. Additionally, treating cells with serum-free media is simple and does not require additional materials to be purchased. The second factor, Y-27632, is an actin-myosin contractility inhibitor. Specifically, Y-27632 inhibits the formation of cytoskeletal fibers which regulate cell shape and propulsive force [77, 82]. This factor has been shown to reduce adhesion strength [77] and inhibit microtissue release from swelling microbeams [83]; both of which could correspond to a decrease in stiffness. The third factor, nocodazole, depolymerizes microtubules within the cytoskeleton. Microtubules are thought to balance contractile elements within the cell and have been shown to regulate cell adhesion strength via cell shape [42]. If microtubules balance contractile elements and provide resistance to compression, then exposing the cell to nocodazole should increase the cell's compressibility, resulting in a decrease in cellular stiffness. The final factor, sodium azide, is a potent ATP production inhibitor [84]. Specifically, sodium azide inhibits cytochrome C oxidase in mitochondria to block ATP production. ATP is known as the energy unit of the cell and is used by many cellular processes including the formation of structural proteins. Without ATP production many of the cell's structural components will cease to function, leading to the hypothesis that cellular stiffness will decrease when exposed to this factor.

## References

- [1] J. Rouwkema, N. C. Rivron, and C. A. van Blitterswijk, "Vascularization in tissue engineering," *Trends in Biotechnology*, vol. 26, pp. 434-441, 2008/08/01/ 2008.
- [2] R. K. Jain, P. Au, J. Tam, D. G. Duda, and D. Fukumura, "Engineering vascularized tissue," *Nature Biotechnology*, vol. 23, pp. 821-823, 2005/07/01 2005.
- [3] L. Gui and L. E. Niklason, "Vascular Tissue Engineering: Building Perfusable Vasculature for Implantation," *Current opinion in chemical engineering*, vol. 3, pp. 68-74, 2014.
- [4] S. L. M. Dahl, C. Rhim, Y. C. Song, and L. E. Niklason, "Mechanical properties and compositions of tissue engineered and native arteries," *Annals of biomedical engineering*, vol. 35, pp. 348-355, 2007.
- [5] T. N. McAllister, M. Maruszewski, S. A. Garrido, W. Wystrychowski, N. Dusserre, A. Marini, *et al.*, "Effectiveness of haemodialysis access with an autologous tissue-engineered vascular graft: a multicentre cohort study," *Lancet*, vol. 373, pp. 1440-6, Apr 25 2009.
- [6] M. Evander, L. Johansson, T. Lilliehorn, J. Piskur, M. Lindvall, S. Johansson, *et al.*, "Noninvasive Acoustic Cell Trapping in a Microfluidic Perfusion System for Online Bioassays," *Analytical Chemistry*, vol. 79, pp. 2984-2991, 2007/04/01 2007.
- [7] X. Ding, S.-C. S. Lin, B. Kiraly, H. Yue, S. Li, I.-K. Chiang, *et al.*, "On-chip manipulation of single microparticles, cells, and organisms using surface acoustic waves," *Proceedings of the National Academy of Sciences*, vol. 109, pp. 11105-11109, July 10, 2012 2012.
- [8] A. Haake, A. Neild, D.-H. Kim, J.-E. Ihm, Y. Sun, J. Dual, *et al.*, "Manipulation of cells using an ultrasonic pressure field," *Ultrasound in Medicine & Biology*, vol. 31, pp. 857-864, 6// 2005.
- [9] M. C. Jo and R. Guldiken, "Particle manipulation by phase-shifting of surface acoustic waves," *Sensors and Actuators A: Physical*, vol. 207, pp. 39-42, 3/1/ 2014.
- [10] K. Yosioka and Y. Kawasima, "Acoustic radiation pressure on a compressible sphere," *Acta Acustica united with Acustica*, vol. 5, pp. 167-173, // 1955.
- [11] S.-Y. Tee, J. Fu, Christopher S. Chen, and Paul A. Janmey, "Cell Shape and Substrate Rigidity Both Regulate Cell Stiffness," *Biophysical Journal*, vol. 100, pp. L25-L27, 3/2/ 2011.
- [12] T. G. Kuznetsova, M. N. Starodubtseva, N. I. Yegorenkov, S. A. Chizhik, and R. I. Zhdanov, "Atomic force microscopy probing of cell elasticity," *Micron*, vol. 38, pp. 824-833, 12// 2007.
- [13] K. D. Costa, A. J. Sim, and F. C. P. Yin, "Non-Hertzian Approach to Analyzing Mechanical Properties of Endothelial Cells Probed by Atomic Force Microscopy," *Journal of Biomechanical Engineering*, vol. 128, pp. 176-184, 2005.
- [14] A. B. Mathur, G. A. Truskey, and W. M. Reichert, "Atomic force and total internal reflection fluorescence microscopy for the study of force transmission in endothelial cells," *Biophysical Journal*, vol. 78, pp. 1725-1735, 2000.
- [15] P. Gascoyne, J. Satayavivad, and M. Ruchirawat, "Microfluidic approaches to malaria detection," *Acta Trop*, vol. 89, pp. 357-69, Feb 2004.
- [16] A. Garcia and N. Gallant, "Stick and grip," *Cell Biochemistry and Biophysics*, vol. 39, pp. 61-73, 2003/08/01 2003.
- [17] S. Moon, U. A. Gurkan, J. Blander, W. W. Fawzi, S. Aboud, F. Mugusi, *et al.*, "Enumeration of CD4+ T-cells using a portable microchip count platform in Tanzanian HIV-infected patients," *PLoS One*, vol. 6, p. e21409, 2011.

- [18] H. Mohamed, M. Murray, J. N. Turner, and M. Caggana, "Isolation of tumor cells using size and deformation," *Journal of Chromatography A*, vol. 1216, pp. 8289-8295, 11/20/ 2009.
- [19] E. E. Hui and S. N. Bhatia, "Micromechanical control of cell-cell interactions," *Proceedings of the National Academy of Sciences*, vol. 104, pp. 5722-5726, April 3, 2007 2007.
- [20] M. C. Jo and R. Guldiken, "Active density-based separation using standing surface acoustic waves," *Sensors and Actuators A: Physical*, vol. 187, pp. 22-28, 11// 2012.
- [21] M. C. Jo and R. Guldiken, "Dual surface acoustic wave-based active mixing in a microfluidic channel," *Sensors and Actuators A: Physical*, vol. 196, pp. 1-7, 7/1/ 2013.
- [22] F. Guo, P. Li, J. B. French, Z. M. Mao, H. Zhao, S. X. Li, *et al.*, "Controlling cell-cell interactions using surface acoustic waves," *Proceedings of the National Academy of Sciences of the United States of America*, vol. 112, pp. 43-48, Jan 6 2015.
- [23] C. Poon, D. McMahon, and K. Hynynen, "Noninvasive and targeted delivery of therapeutics to the brain using focused ultrasound," *Neuropharmacology*, vol. 120, pp. 20-37, 2017/07/01/ 2017.
- [24] Y.-J. R. Chang, J. Perry, and K. Cross, "Low-Frequency Ultrasound Debridement in Chronic Wound Healing: A Systematic Review of Current Evidence," *Plastic surgery (Oakville, Ont.)*, vol. 25, pp. 21-26, 2017.
- [25] T. van Rooij, I. Skachkov, I. Beekers, K. R. Lattwein, J. D. Voorneveld, T. J. A. Kokhuis, *et al.*, "Viability of endothelial cells after ultrasound-mediated sonoporation: Influence of targeting, oscillation, and displacement of microbubbles," *Journal of Controlled Release*, vol. 238, pp. 197-211, 2016/09/28/ 2016.
- [26] D. Bani, A. Quattrini Li, G. Freschi, and G. L. Russo, "Histological and Ultrastructural Effects of Ultrasound-induced Cavitation on Human Skin Adipose Tissue," *Plastic and reconstructive surgery. Global open*, vol. 1, pp. e41-e41, 2013.
- [27] D. L. Miller, N. B. Smith, M. R. Bailey, G. J. Czarnota, K. Hynynen, I. R. S. Makin, *et al.*, "Overview of therapeutic ultrasound applications and safety considerations," *Journal of ultrasound in medicine : official journal of the American Institute of Ultrasound in Medicine*, vol. 31, pp. 623-634, 2012.
- [28] J. Voigt, M. Wendelken, V. Driver, and O. M. Alvarez, "Low-frequency ultrasound (20-40 kHz) as an adjunctive therapy for chronic wound healing: a systematic review of the literature and meta-analysis of eight randomized controlled trials," *Int J Low Extrem Wounds*, vol. 10, pp. 190-9, Dec 2011.
- [29] O. Doblhoff-Dier, T. Gaida, H. Katinger, W. Burger, M. Groschl, and E. Benes, "A novel ultrasonic resonance field device for the retention of animal cells," *Biotechnol Prog*, vol. 10, pp. 428-32, Jul-Aug 1994.
- [30] S. Radel, A. J. McLoughlin, L. Gherardini, O. Doblhoff-Dier, and E. Benes, "Viability of yeast cells in well controlled propagating and standing ultrasonic plane waves," *Ultrasonics*, vol. 38, pp. 633-637, 3// 2000.
- [31] J. Hultström, O. Manneberg, K. Dopf, H. M. Hertz, H. Brismar, and M. Wiklund, "Proliferation and viability of adherent cells manipulated by standing-wave ultrasound in a microfluidic chip," *Ultrasound in Medicine & Biology*, vol. 33, pp. 145-151, 1// 2007.
- [32] F. W. Kremkau, "Cancer therapy with ultrasound: A historical review," *Journal of Clinical Ultrasound*, vol. 7, pp. 287-300, 1979.
- [33] J. A. Newell, "Ultrasonics in Medicine," *Physics in Medicine and Biology*, vol. 8, pp. 241-264, 1963/09/01 1963.
- [34] M. Dyson, B. Woodward, and J. B. Pond, "Flow of Red Blood Cells stopped by Ultrasound," *Nature*, vol. 232, pp. 572-573, 08/20/print 1971.

- [35] M. Dyson, J. B. Pond, B. Woodward, and J. Broadbent, "The production of blood cell stasis and endothelial damage in the blood vessels of chick embryos treated with ultrasound in a stationary wave field," *Ultrasound in Medicine & Biology*, vol. 1, pp. 133-148, 3// 1974.
- [36] R. Guldiken, M. C. Jo, N. D. Gallant, U. Demirci, and J. Zhe, "Sheathless Size-Based Acoustic Particle Separation," *Sensors*, vol. 12, pp. 905-922, 2012.
- [37] F. Petersson, A. Nilsson, C. Holm, H. Jonsson, and T. Laurell, "Separation of lipids from blood utilizing ultrasonic standing waves in microfluidic channels," *Analyst*, vol. 129, pp. 938-943, 2004.
- [38] N. D. Gallant, K. E. Michael, and A. J. García, "Cell Adhesion Strengthening: Contributions of Adhesive Area, Integrin Binding, and Focal Adhesion Assembly," *Molecular Biology of the Cell*, vol. 16, pp. 4329-4340, September 1, 2005 2005.
- [39] N. D. Gallant and A. J. García, "Model of integrin-mediated cell adhesion strengthening," *Journal of Biomechanics*, vol. 40, pp. 1301-1309, // 2007.
- [40] J. C. Bischof, J. Padanilam, W. H. Holmes, R. M. Ezzell, R. C. Lee, R. G. Tompkins, *et al.*, "Dynamics of cell membrane permeability changes at suprphysiological temperatures," *Biophys J*, vol. 68, pp. 2608-14, Jun 1995.
- [41] M. M. Roden, K.-H. Lee, M. C. Panelli, and F. M. Marincola, "A novel cytolysis assay using fluorescent labeling and quantitative fluorescent scanning technology," *Journal of Immunological Methods*, vol. 226, pp. 29-41, 6/24/ 1999.
- [42] K. Elineni and N. Gallant, "Microtubules Mechanically Regulate Cell Adhesion Strengthening Via Cell Shape," *Cellular and Molecular Bioengineering*, vol. 7, pp. 136-144, 2014/03/01 2014.
- [43] M. Incorporated. (04/03/2020). *Sonicator 3000 Ultrasonic Liquid Processor Operation Manual*. Available: [https://archive-resources.coleparmer.com/Manual\\_pdfs/04711-xxMisonix3000.pdf](https://archive-resources.coleparmer.com/Manual_pdfs/04711-xxMisonix3000.pdf)
- [44] P. Y. Chiou, A. T. Ohta, and M. C. Wu, "Massively parallel manipulation of single cells and microparticles using optical images," *Nature*, vol. 436, pp. 370-2, Jul 21 2005.
- [45] M. L. Jewell, N. J. Solish, and C. S. Desilets, "Noninvasive body sculpting technologies with an emphasis on high-intensity focused ultrasound," *Aesthetic Plast Surg*, vol. 35, pp. 901-12, Oct 2011.
- [46] R. A. Wong, B. Schumann, R. Townsend, and C. A. Phelps, "A survey of therapeutic ultrasound use by physical therapists who are orthopaedic certified specialists," *Phys Ther*, vol. 87, pp. 986-94, Aug 2007.
- [47] M. Wiklund, "Acoustofluidics 12: Biocompatibility and cell viability in microfluidic acoustic resonators," *Lab Chip*, vol. 12, pp. 2018-28, May 8 2012.
- [48] D. Debavelaere-Callens, L. Peyre, P. Campistron, and H. F. Hildebrand, "On the use of ultrasounds to quantify the longitudinal threshold force to detach osteoblastic cells from a conditioned glass substrate," *Biomolecular Engineering*, vol. 24, pp. 521-525, 11// 2007.
- [49] N. J. Hangiandreou, "AAPM/RSNA physics tutorial for residents: Topics in US - B-mode US: Basic concepts and new technology," *Radiographics*, vol. 23, pp. 1019-1033, Jul-Aug 2003.
- [50] F. J. Trujillo and K. Knoerzer, "A computational modeling approach of the jet-like acoustic streaming and heat generation induced by low frequency high power ultrasonic horn reactors," *Ultrasonics Sonochemistry*, vol. 18, pp. 1263-1273, 2011/11/01/ 2011.
- [51] I. Lentacker, I. De Cock, R. Deckers, S. C. De Smedt, and C. T. Moonen, "Understanding ultrasound induced sonoporation: definitions and underlying mechanisms," *Adv Drug Deliv Rev*, vol. 72, pp. 49-64, Jun 2014.
- [52] I. Tzanakis, G. S. B. Lebon, D. G. Eskin, and K. A. Pericleous, "Characterizing the cavitation development and acoustic spectrum in various liquids," *Ultrasonics Sonochemistry*, vol. 34, pp. 651-662, 2017/01/01/ 2017.
- [53] R. S. (London), *Philosophical Transactions of the Roday Society of London Volume 121*, 1831.

- [54] Thermofisher. (2020). *CellTracker fluorescent probes Product Information Sheet*. Available: [https://assets.thermofisher.com/TFS-Assets/LSG/manuals/MAN0001826\\_CellTracker\\_Probes\\_PI.pdf](https://assets.thermofisher.com/TFS-Assets/LSG/manuals/MAN0001826_CellTracker_Probes_PI.pdf)
- [55] Thermofisher. *LIVE/DEAD® Viability/Cytotoxicity Kit*. Available: <https://assets.thermofisher.com/TFS-Assets/LSG/manuals/mp03224.pdf>
- [56] W. Xu, R. Mezencev, B. Kim, L. Wang, J. McDonald, and T. Sulchek, "Cell Stiffness Is a Biomarker of the Metastatic Potential of Ovarian Cancer Cells," *PLoS ONE*, vol. 7, p. e46609, 2012.
- [57] J. M. MITCHISON and M. M. SWANN, "The Mechanical Properties of the cell Surface," *II. The Unfertilized Sea-Urchin Egg*, vol. 31, pp. 461-472, 1954.
- [58] R. P. Rand and A. C. Burton, "Mechanical Properties of the Red Cell Membrane," *Biophysical Journal*, vol. 4, pp. 115-135, 1964/03/01 1964.
- [59] C. Dong, R. Skalak, K. L. Sung, G. W. Schmid-Schonbein, and S. Chien, "Passive deformation analysis of human leukocytes," *Journal of Biomechanical Engineering*, vol. 110, pp. 27-41, 1988.
- [60] A. Ashkin, "Acceleration and Trapping of Particles by Radiation Pressure," *Physical Review Letters*, vol. 24, pp. 156-159, 01/26/ 1970.
- [61] A. Ashkin and J. Dziedzic, "Optical trapping and manipulation of viruses and bacteria," *Science*, vol. 235, pp. 1517-1520, 1987.
- [62] J. Guck, R. Ananthakrishnan, T. J. Moon, C. C. Cunningham, and J. Käs, "Optical Deformability of Soft Biological Dielectrics," *Physical Review Letters*, vol. 84, pp. 5451-5454, 06/05/ 2000.
- [63] B. Jagannathan and S. Marqusee, "Protein Folding and Unfolding Under Force," *Biopolymers*, vol. 99, pp. 860-869, 2013.
- [64] N. Wang, J. P. Butler, and D. E. Ingber, "Mechanotransduction across the cell surface and through the cytoskeleton," *Science*, vol. 260, pp. 1124-7, May 21 1993.
- [65] G. Binnig, C. F. Quate, and C. Gerber, "Atomic force microscope," *Physical review letters*, vol. 56, p. 930, 1986.
- [66] J. Helenius, C.-P. Heisenberg, H. E. Gaub, and D. J. Muller, "Single-cell force spectroscopy," *Journal of Cell Science*, vol. 121, pp. 1785-1791, June 1, 2008 2008.
- [67] J. Friedrichs, K. R. Legate, R. Schubert, M. Bharadwaj, C. Werner, D. J. Muller, *et al.*, "A practical guide to quantify cell adhesion using single-cell force spectroscopy," *Methods*, vol. 60, pp. 169-78, Apr 1 2013.
- [68] H. Xie, M. Yin, W. Rong, and L. Sun, "In Situ Quantification of Living Cell Adhesion Forces: Single Cell Force Spectroscopy with a Nanotweezer," *Langmuir*, vol. 30, pp. 2952-2959, 2014/03/18 2014.
- [69] P. V. Zinin, J. S. Allen, and V. M. Levin, "Mechanical resonances of bacteria cells," *Physical Review E*, vol. 72, p. 061907, 12/12/ 2005.
- [70] M. M. Zarandi, A. Bonakdar, and I. Stiharu, "Investigations on natural frequencies of individual spherical and ellipsoidal bakery yeast cells."
- [71] H. Wee and A. Voloshin, "Modal analysis of a spreading osteoblast cell in culturing," in *2012 38th Annual Northeast Bioengineering Conference (NEBEC)*, 2012, pp. 167-168.
- [72] S. K. Jaganathan, A. P. Subramanian, M. V. Vellayappan, A. Balaji, A. A. John, A. K. Jaganathan, *et al.*, "Natural frequency of cancer cells as a starting point in cancer treatment," *Current Science*, vol. 110, pp. 1828-1832, 2016.
- [73] A. Geltmeier, B. Rinner, D. Bade, K. Meditz, R. Witt, U. Bicker, *et al.*, "Characterization of Dynamic Behaviour of MCF7 and MCF10A Cells in Ultrasonic Field Using Modal and Harmonic Analyses," *PLOS ONE*, vol. 10, p. e0134999, 2015.
- [74] T. Fukuda, M. Nakajima, H. Tajima, S. Yajing, and Y. Tao, "Micro-nanomanipulation system toward biological cell analysis and assembly," in *Innovative Engineering Systems (ICIES), 2012 First International Conference on*, 2012, pp. 31-36.

- [75] T. Fukuda, M. Nakajima, L. Pou, and M. R. Ahmad, "Bringing the nanolaboratory inside electron microscopes," *Nanotechnology Magazine, IEEE*, vol. 2, pp. 18-31, 2008.
- [76] Kranthi K. Elineni and Nathan D. Gallant, "Regulation of Cell Adhesion Strength by Peripheral Focal Adhesion Distribution," *Biophysical Journal*, vol. 101, pp. 2903-2911, 05/30/received 11/09/accepted 2011.
- [77] D. W. Dumbauld, H. Shin, N. D. Gallant, K. E. Michael, H. Radhakrishna, and A. J. Garcia, "Contractility modulates cell adhesion strengthening through focal adhesion kinase and assembly of vinculin-containing focal adhesions," *J Cell Physiol*, vol. 223, pp. 746-56, Jun 2010.
- [78] N. A. Burnham, X. Chen, C. S. Hodges, G. A. Matei, E. J. Thoreson, C. J. Roberts, *et al.*, "Comparison of calibration methods for atomic-force microscopy cantilevers," *Nanotechnology*, vol. 14, p. 1, 2003.
- [79] S. M. Cook, T. E. Schäffer, K. M. Chynoweth, M. Wigton, R. W. Simmonds, and K. M. Lang, "Practical implementation of dynamic methods for measuring atomic force microscope cantilever spring constants," *Nanotechnology*, vol. 17, p. 2135, 2006.
- [80] I. M. Malovichko, "Measuring AFM cantilever stiffness from a thermal noise spectrum," *Bulletin of the Russian Academy of Sciences: Physics*, vol. 77, pp. 972-974, 2013/08/01 2013.
- [81] Y. Shen, M. Nakajima, Z. Yang, H. Tajima, Z. Najdovski, M. Homma, *et al.*, "Single cell stiffness measurement at various humidity conditions by nanomanipulation of a nano-needle," *Nanotechnology*, vol. 24, p. 145703, Apr 12 2013.
- [82] T. Ishizaki, M. Uehata, I. Tamechika, J. Keel, K. Nonomura, M. Maekawa, *et al.*, "Pharmacological properties of Y-27632, a specific inhibitor of rho-associated kinases," *Mol Pharmacol*, vol. 57, pp. 976-83, May 2000.
- [83] O. O. Akintewe, S. J. DuPont, K. K. Elineni, M. C. Cross, R. G. Toomey, and N. D. Gallant, "Shape-changing hydrogel surfaces trigger rapid release of patterned tissue modules," *Acta Biomaterialia*.
- [84] F. Palmieri and M. Klingenberg, "Inhibition of Respiration under the Control of Azide Uptake by Mitochondria," in *European Journal of Biochemistry*, C. Liébecq, Ed., ed: Springer Berlin Heidelberg, 1967, pp. 439-446.

## **Appendix A Copyright Permissions**

There are no copyright permissions needed.